

2

Study of an embarked vibro-impact system: experimental analysis

This chapter presents and discusses the experimental part of the thesis. Two test rigs were built at the Dynamics and Vibrations laboratory at PUC-Rio. The test rigs have the purpose of representing the axial movement performed by the drillstring bottom hole assembly and explaining the impact phenomenon when such forces occurred in an embarked system. The expected results of this test rig include obtaining the hammer characteristics, i.e., the range of possible excitation frequencies and impulsive force measurements. The hammer is composed of an impact mass and beam springs. In order to isolate the influence of each component on the impact force behavior, a previous experiment was performed. In this experiment the hammer is supported by wires. Previous experiments have shown that a hammer configuration with beam springs introduces nonlinearities which make parameter identification difficult, demanding more complex analytical model for the numerical results [2].

2.1

First experiment - hammer supported by wires

2.1.1

Experimental apparatus

This experimental apparatus, shown in Figure 2.1, was designed to represent the drillstring axial behavior and its influence over the impact device (hammer).

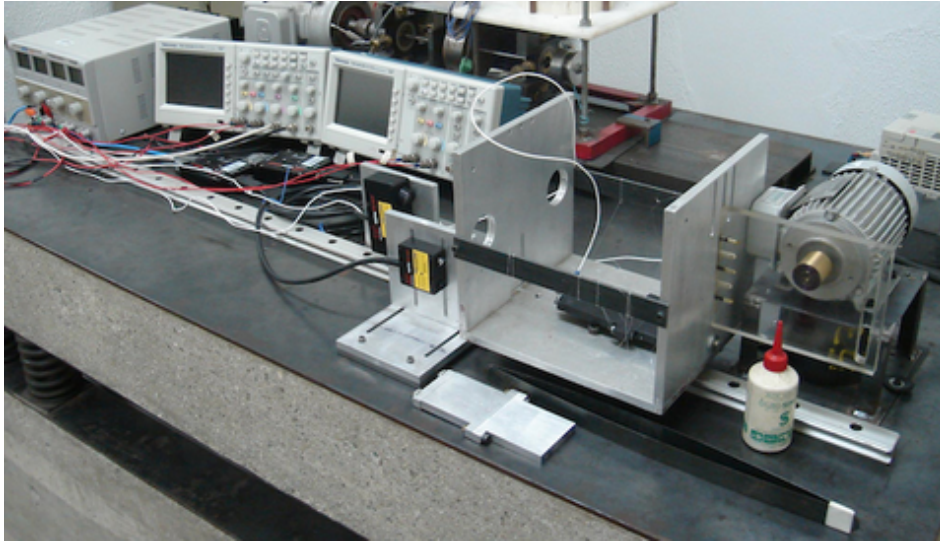


Figure 2.1: First test rig: hammer supported by wires. Picture of the entire test rig, including acquisition hardware.

The experiment consists of a main cart, made of aluminum, which slides along the horizontal axis on a low friction rail bearing assembly (INA-Laufwagen LFL52-E-SF). The main cart is excited by an inverter controlled AC motor (EBERLE model B56b4, 745.7 W). The motor is attached to the cart through a pin that slides into a slot machined on an acrylic plate attached to the cart. The pin hole is drilled off-centered on the disk at the edge of the motor, so that rotational motor movement becomes sinusoidal cart movement. This device is used instead of an electromagnetic shaker because it can perform higher hammer amplitudes than a shaker. The device also avoids the influence of impact forces on the excitation source at higher frequencies. This is an improvement gained in previous experimental set-ups [3].

The hammer is fixed inside the main cart, Figure 2.3(a), its weight supported by nylon wires. The entire system moves in a horizontal axis. As shown in Figures 2.1 and 2.3, eight nylon wires are used, assuring that the hammer moves in the same axis as the main cart. The wires are attached to the cart structure at an angle of 30 degrees approximately from the vertical axis, to minimize hammer rotation after impact. The hammer is composed of aluminum with a steel impact device. To vary the gap between the hammer and the cart, the impact device is composed of a screw and a knurled nut, as shown in Figure 2.3(b). The measurement devices on the test rig include:

- one accelerometer attached to the hammer (accelerometer Endevco 751-10 SN AC69);

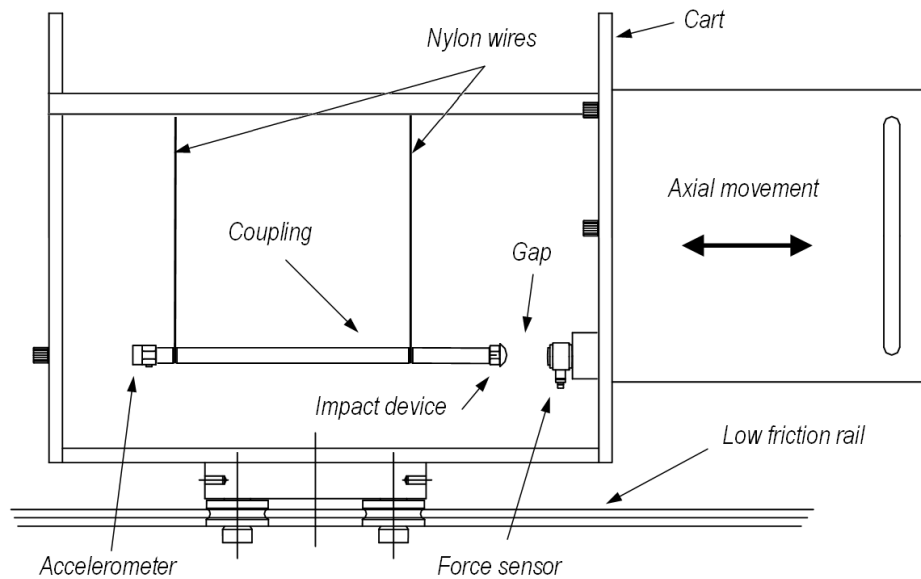


Figure 2.2: First test rig: cart and hammer sketch.

- one piezoelectric force sensor (Endevco 2311-100 SN 2471), fixed to the cart and located in front of the hammer impact device;
- two laser displacement sensors, both located on the side of the cart. One of the laser displacement sensors measures cart displacement (optoNCDT 1607-20) and the other measures hammer displacement (optoNCDT 1607-100). Both laser displacement sensors are DC powered (ICEL power supply PS-500).

The accelerometer signal is filtered by a signal conditioner (ENDEVCO Isotron 2792B). The force sensor is powered and its signal filtered by an ICP signal conditioner (PCB 482C05). All data is acquired by two oscilloscopes (Tektronix digital storage oscilloscopes) that use different time scales. The first oscilloscope (TDS 2024B) measures the impact force and acceleration at the precise moment of impact (micro scale), after the impact force signal is triggered. The second oscilloscope (TDS 2012B) measures both cart and hammer displacements using laser displacement sensors signals (macro scale).

2.1.2 Experimental methodology

The inputs are the gap and the excitation frequency. The length of the gap is measured using a calibrated shim. The excitation frequency is supplied by the AC motor. The outputs are: the acceleration signal from

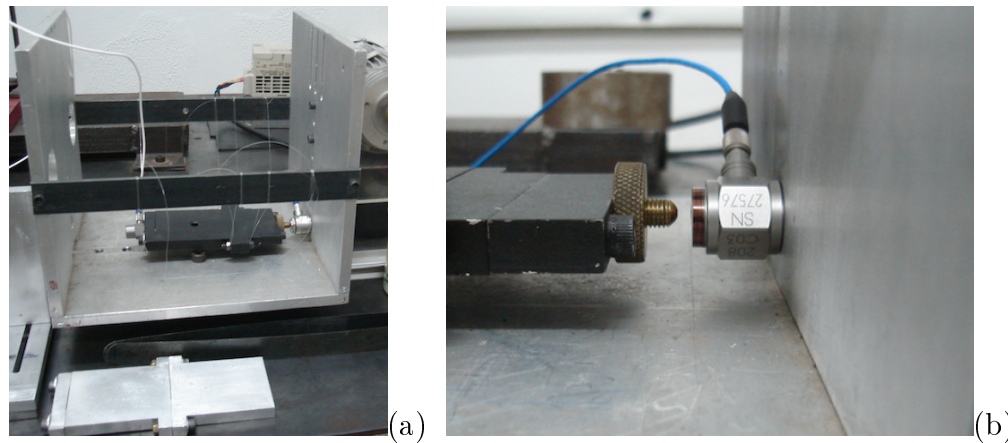


Figure 2.3: First test rig photos: a) Detail of cart and hammer; b) Impact gap device, composed by knurled nut and screw.

the accelerometer mounted on the top of the hammer; the impact force applied by the hammer; the cart and hammer displacements.

As in previous experiment [2] [3] [4], the methodology here is to observe the impact force behavior as the gap is varied. First, the natural frequency of the system without impact is determined, as well as the system parameters. After that, a study with impact is carried out. The excitation frequency is varied in order to cover the possible range of excitation frequencies. Three different gap values were chosen: 0.0 mm, 1.0 mm and 2.4 mm.

The laser displacement sensor signal presents an undesirable level of noise, which was removed using a moving average filter. In statistics, a moving average is used to analyze a set of data points by creating a series of averages of different subsets of the full data set [90]. The size of the subset being averaged is always constant, always being compared to the original signal so no relevant phenomena is masked. After the filtered signal is differentiated to obtain the hammer velocity, then the phase plane can be plotted. Due to the nature of the moving average (a low-pass filter) the phase plane charts show a smooth effect during the impact, which is an effect of the differentiation of low-pass filtered signal, and does not reflect the reality of the impact, as will be seen during the comparison between experimental data and numerical results.

2.1.3

Experimental Results for no impact ($\text{gap} \rightarrow \infty$)

If there is no impact, the hammer behaves as a one-degree-of-freedom system excited by a harmonic load (in this case, a base excitation), even

Table 2.1: First experiment. Sensor specs.

Cart Accelerometer - 751-10 SN AC69		
Sensitivity	10.194	mV/g
Measure Range	± 50	g
Resonance frequency	50	kHz
Impact Force Sensor - 2311-100 SN 2471		
Sensitivity	24.41	mV/N
Measure Range	± 220	N
Resonance frequency	75	kHz
Cart laser displacement sensor - optoNCDT 1607-20		
Sensitivity	10	V/mm
Measure Range	20	mm
Hammer laser displacement sensor - optoNCDT 1607-100		
Sensitivity	2	V/mm
Measure Range	100	mm

showing the *beat* phenomenon [42]. Since such system is well known and widely described in literature [26] [42], it warrants no further comments. The charts showing the beat phenomenon as well as the system frequency response are shown in Figure 2.4.

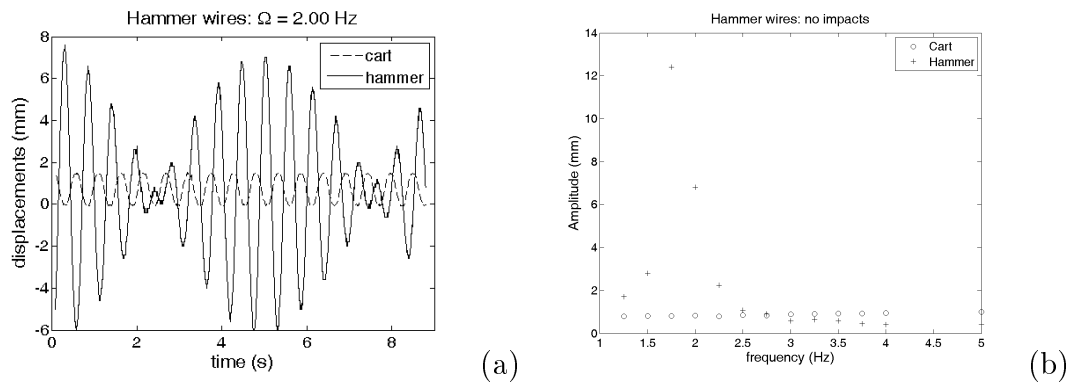


Figure 2.4: Hammer supported by wires. No impact: a) Beat, excitation frequency 2.00 Hz; b) Frequency response.

2.1.4 Experimental Results for gap 0.0mm

As noted in the previous experiment [2], hammer impact force behavior can be split into frequency bands, showing similar characteristics in each frequency band for all gaps.

In a low excitation frequency range (less than 2.5 Hz), the cart movement is so slow that the hammer basically follows the prescribed excitation, generating two or three impacts per excitation cycle with low force magnitude. Due to the low impact force magnitude produced, such frequency range is not discussed in this work. In the next level of frequencies, the impact force presents a period-1 ($z = 1/1$, 1 impact per 1 excitation cycle) stable behavior. The impact force magnitude increases as the excitation frequency increases, reaching its highest value at 3.75 Hz (82.4 N) and after this frequency the impact force decreases as the frequency is raised. Figures 2.5 and 2.6 show the impact force, hammer acceleration and both cart and hammer absolute displacements for the maximum impact force of frequency band $z = 1/1$. The impact force transducer captures the first impulse transferred by the hammer, reaching its maximum. After the first impulse, in the micro scale time analysis, the support structure bounces back transferring energy to the hammer. The contact dynamics reacts according to its own dynamics, reaching a second peak at around 50 N. The accelerometer measures the hammer dynamics, because it is fixed to the opposite side of the impact device, see Figure 2.2. The existence of contact dynamics is strengthened by the results shown in the acceleration chart, because there are unexpected oscillations after the impact. This could lead to the hypothesis that the hammer has an axial vibration behavior that is relevant to the impact process.

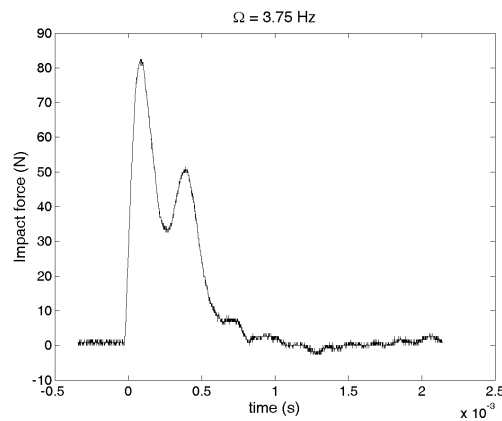


Figure 2.5: Hammer supported by wires. Gap 0.0 mm. Excitation frequency 3.75Hz. Impact force over time.

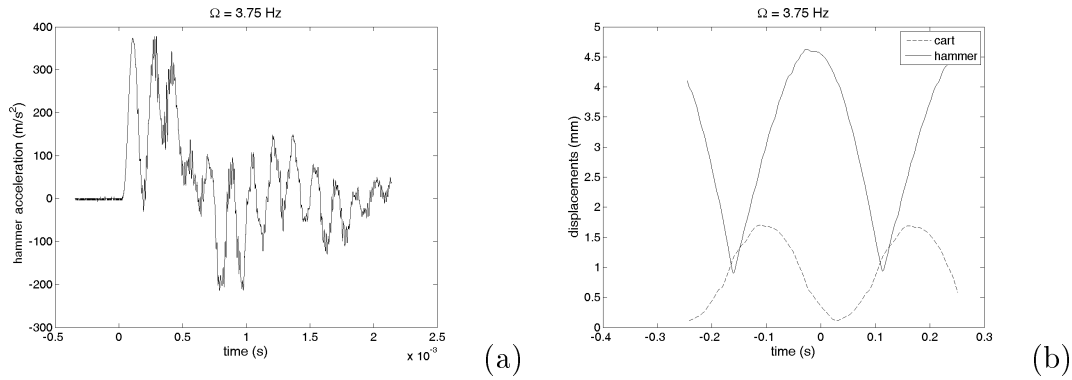


Figure 2.6: Hammer supported by wires. Gap 0.0 mm. Excitation frequency 3.75Hz. Impact force over time; hammer acceleration over time; displacements (cart and hammer)

At the end of frequency band $z = 1/1$, the hammer presents a bifurcation in the impact force behavior, characterized by a period-1 impact with low magnitudes at alternate impact magnitudes, as shown in Figure 2.7.

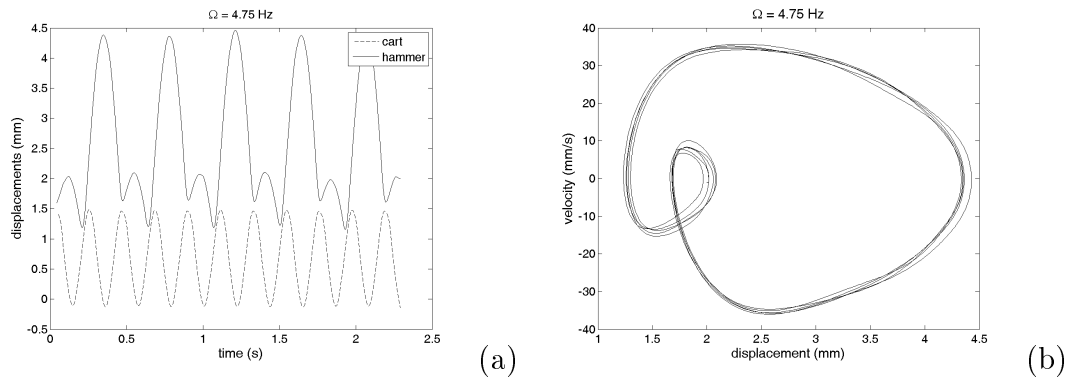


Figure 2.7: Hammer supported by wires. Gap 0.0 mm. Bifurcation. Excitation frequency 4.75 Hz: a) Displacements; b) Hammer phase plane.

The second frequency band presents a similar curve. In this frequency band the impact force occurs every two excitation cycles ($z = 1/2$), with the impact force peak increasing as the frequency increases, reaching its highest value at 7.25 Hz (120 N). The excitation frequency where the maximum impact force occurs on this frequency band ($z = 1/2$) is twice that of frequency band $z = 1/1$. Charts showing the output parameters for the maximum impact force on frequency band $z = 1/2$ are shown in Figures 2.8 and 2.9. After the activity at frequency band $z = 1/2$ the system shows another transitory behavior.

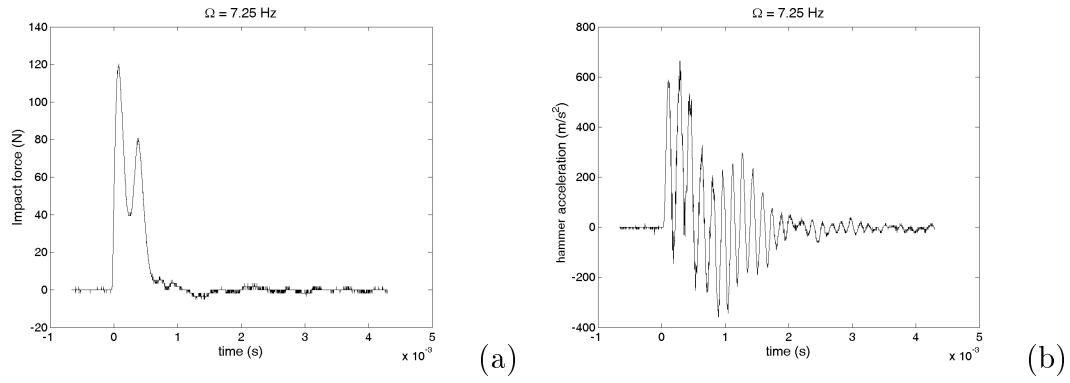


Figure 2.8: Hammer supported by wires. Gap 0.0 mm. Maximum impact force on frequency band $z = 1/2$. Excitation frequency 7.25 Hz: a) Impact force; b) Hammer acceleration.

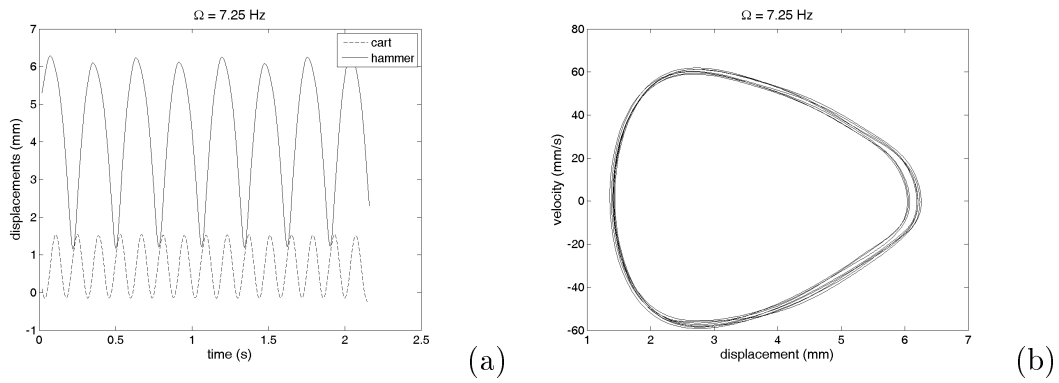


Figure 2.9: Hammer supported by wires. Gap 0.0 mm. Maximum impact force on frequency band $z = 1/2$. Excitation frequency 7.25 Hz: a) Displacements; b) Hammer phase plane.

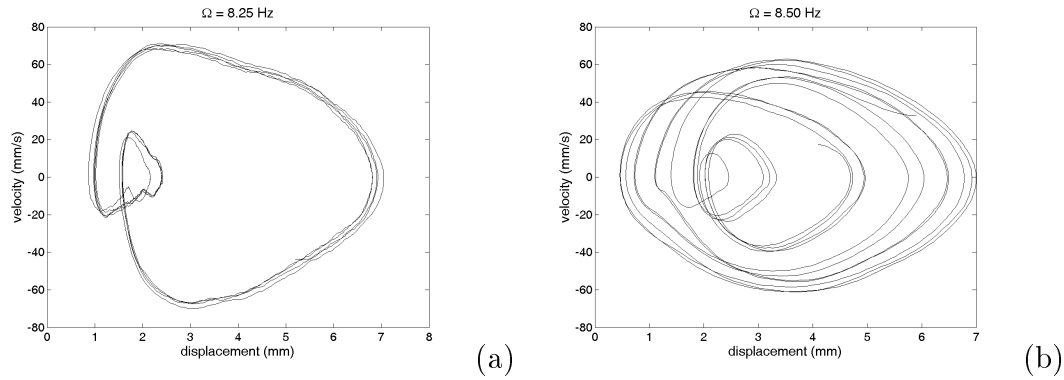


Figure 2.10: Hammer supported by wires. Gap 0.0 mm. Transitory behavior. Hammer phase planes: a) Excitation frequency 8.25 Hz; b) Excitation frequency 8.50 Hz.

Although data was not collected at higher frequencies, what appears to happen is that the frequency bands keep repeating the pattern, with the impact force behavior changing to one impact every three, four, five excitation cycles and so on, always with a bifurcation in between frequency bands. In each frequency band, the excitation frequency where the maximum impact force is found is a multiple of the frequency of the maximum impact force on period-1 ($z = 1/1$).

With this experimental data it is possible to analyze the system behavior in the frequency domain. To do so, a computational routine has been developed to determine the F_i (impact force peak). The maximum value of F_i has been extracted for each excitation frequency. Since the impact force peak does not change within each excitation frequency, except for the behavior after bifurcation, this routine seems to be quite effective. Finally, to generate a non-dimensional chart the force ratio F_i/mg is used (mg is the hammer weight), and the excitation frequency is divided by the natural frequency of the hammer without impact. The natural frequency of the hammer is experimentally identified using modal analysis. This non-dimensional chart will be useful to compare data between different hammer configurations.

Therefore, the impact force ratio chart (F_i/mg) in the frequency domain for this imposed gap is shown in Figure 2.11.

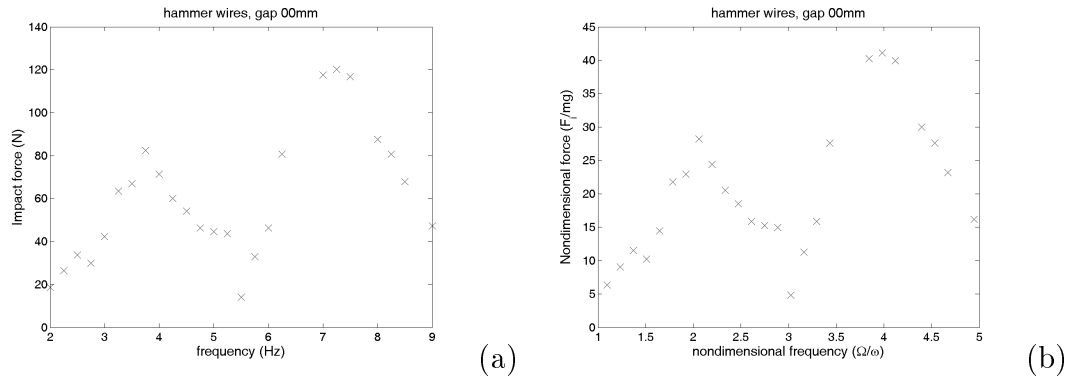


Figure 2.11: Hammer supported by wires. Gap 0.0 mm. Frequency domain response: a) Maximum impact force; b) non-dimensional force, F_i/mg .

Data in Figure 2.11 shows both frequency bands ($z = 1/1$ and $z = 1/2$). Although the maximum impact force on frequency band $z = 1/2$ is higher than frequency band $z = 1/1$, is important to remember that in frequency $z = 1/2$ impacts occur every two cycles and also that energy inserted into the system increases with the square of the excitation frequency. Once the cart displacement is prescribed, the magnitude of the excitation force F_{exc} is:

$$F_{exc} = m_{tot} A_0 \Omega^2, \quad (2-1)$$

where m_{tot} is the total mass (cart and hammer combined), A_0 is the displacement amplitude of the cart and Ω is the excitation frequency.

Using a concept from the linear theory to describe a nonlinear behavior, the excitation frequency where the maximum impact force is achieved is defined as *impact resonance*. Since the hammer displacement is limited by a gap, an interesting phenomenon occurs. The occurrence of the impacts significantly changes the value of the impact resonance, as compared to the hammer resonance, as observed in Table 2.2. This change of resonance in the occurrence of impacts has already been studied [52] and these results were expected.

2.1.5

Experimental Results for gaps 1.0 mm and 2.4 mm

For these gap configurations the experimental results are similar to those observed for gap 0.0 mm. However, the non-zero gap configurations show differences from the results for 0.0 mm gap. For instance, the

occurrence of nonlinear jump was observed after the impact resonance. Another difference includes the appearance of situations of non-impact, due to the non-zero gap (at higher frequencies, for example, where the amplitudes developed are smaller than the gap). Occurrences of nonlinear behavior were also observed and will be discussed in future section of this chapter (see Figure 2.20).

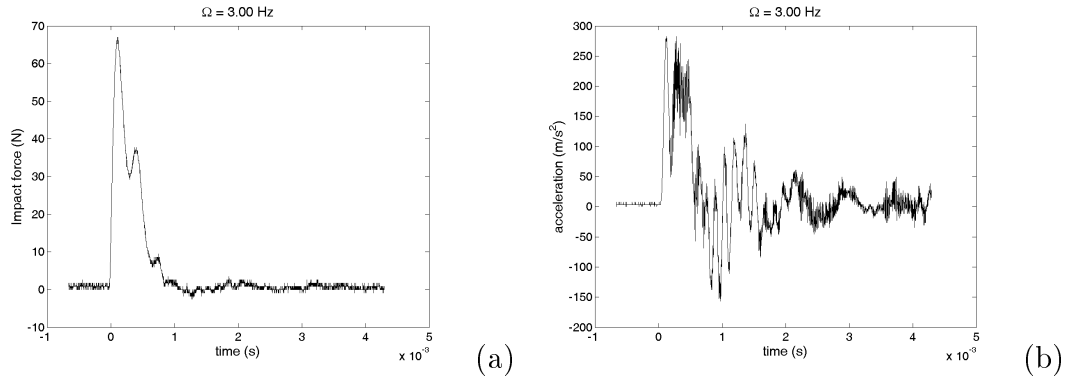


Figure 2.12: Hammer supported by wires. Gap 1.0 mm. Maximum impact force on frequency band $z = 1/1$. Excitation frequency 3.00 Hz: a) Impact force; b) Hammer acceleration.

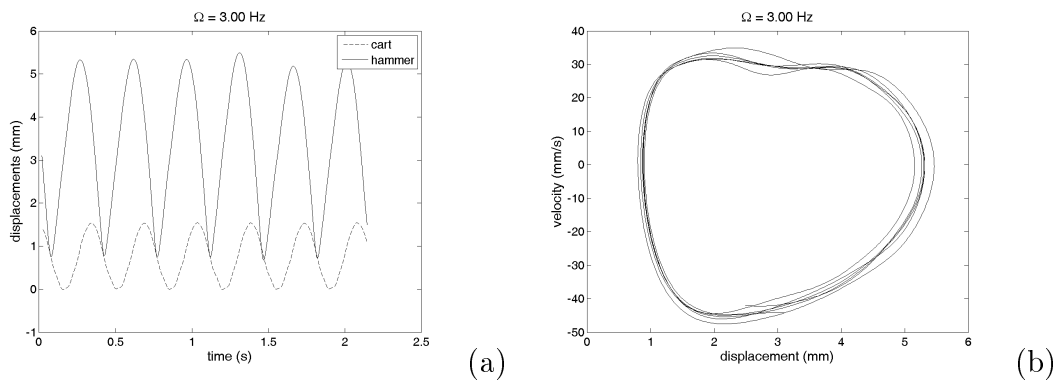


Figure 2.13: Hammer supported by wires. Gap 1.0 mm. Maximum impact force on frequency band $z = 1/1$. Excitation frequency 3.00 Hz: a) Displacements; b) Hammer phase plane.

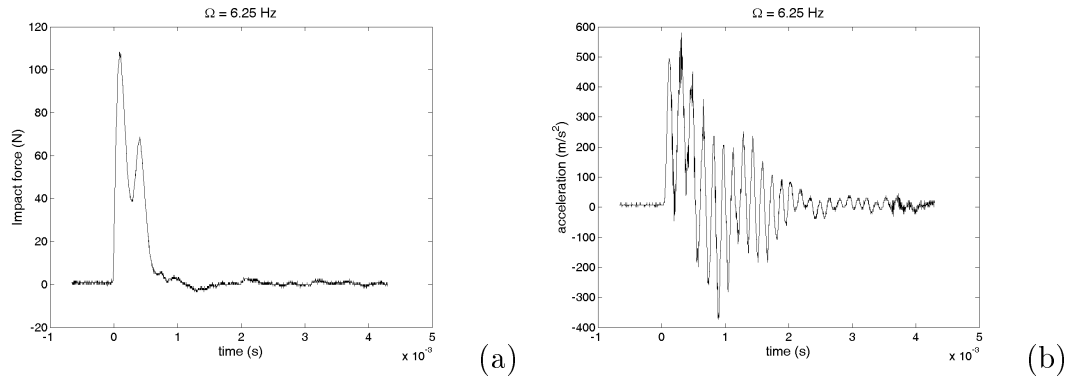


Figure 2.14: Hammer supported by wires. Gap 1.0 mm. Maximum impact force on frequency band $z = 1/2$. Excitation frequency 6.25 Hz: a) Impact force; b) Hammer acceleration.

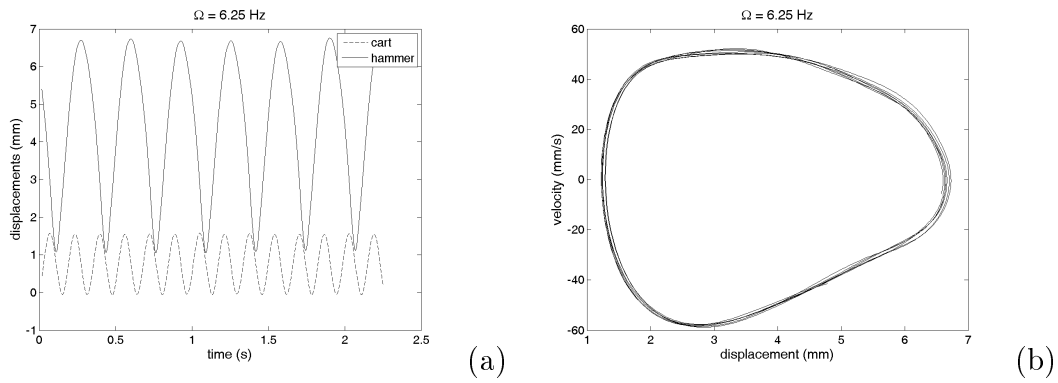


Figure 2.15: Hammer supported by wires. Gap 1.0 mm. Maximum impact force on frequency band $z = 1/2$. Excitation frequency 6.25 Hz: a) Displacements; b) Hammer phase plane.

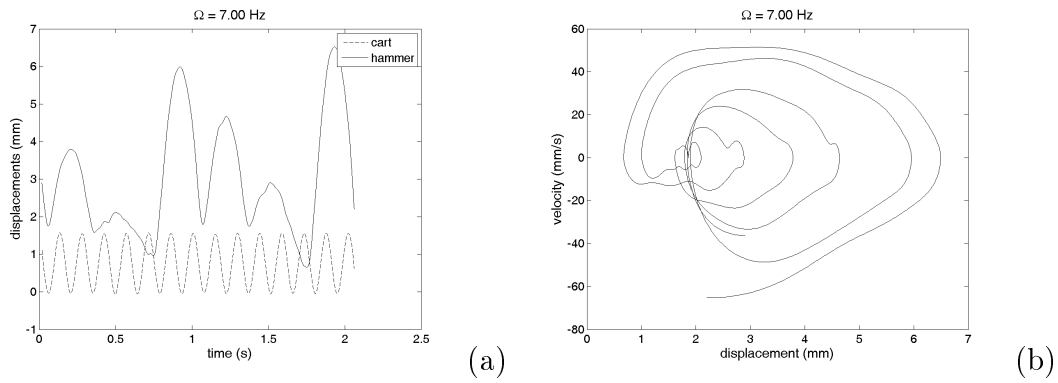


Figure 2.16: Hammer supported by wires. Gap 1.0 mm. Transitory behavior. Excitation frequency 7.00 Hz: a) Displacements; b) Hammer phase plane.

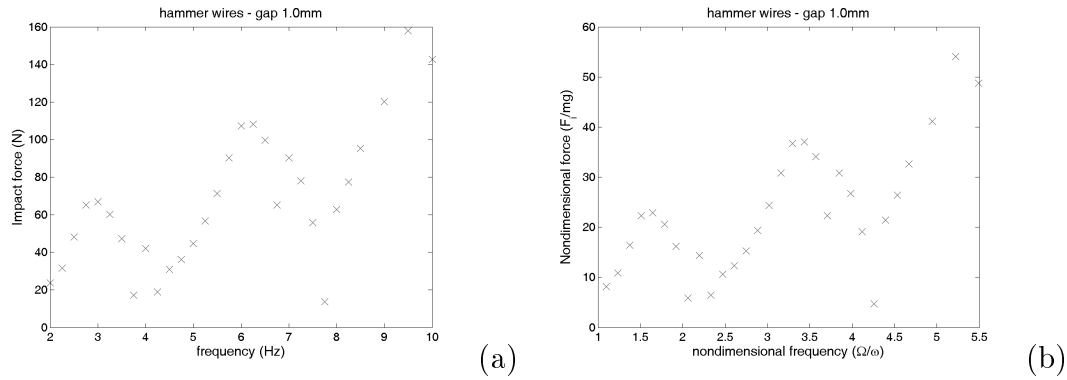


Figure 2.17: Hammer supported by wires. Gap 1.0 mm. Frequency domain response: a) Maximum impact force; b) non-dimensional force, F_i/mg .

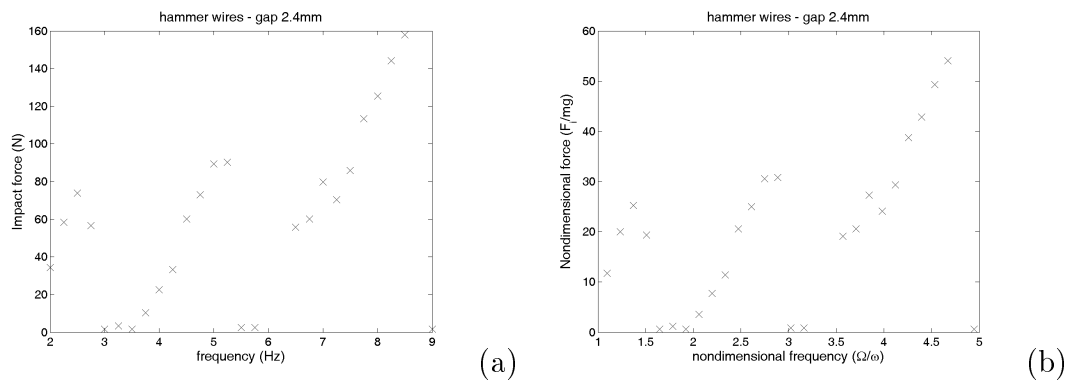


Figure 2.18: Hammer supported by wires. Gap 2.4 mm. Frequency domain response: a) Maximum impact force; b) non-dimensional force, F_i/mg .

2.1.6 Comparison between gap configurations

At this point the charts showing the behavior of the impact force over the excitation for each gap are compared. According to the charts shown in Figure 2.19, for the frequency band $z = 1/1$, the 0.0 mm gap configuration shows the maximum force, but there was no substantial difference for the other gap configurations. For frequency band $z = 1/2$, both gap configurations 0.0 mm and 1.0 mm show the maximum impact force, with the gap 2.4 mm configuration showing the same impact force as in the previous frequency band $z = 1/1$. For possible use in the field, using this hammer set up, it is recommended that the 0.0 mm gap configuration be used, because this configuration shows higher impact force magnitudes. In addition, the 0.0 mm gap configuration shows no occurrence of nonlinear

Table 2.2: Impact resonance frequencies (experimental).

Frequency band	$z = 1/1$ (1 impact/ cycle)	$z = 1/2$ (1 impact/ 2 cycles)
gap 0.0mm	$3.75Hz$	$7.25Hz$
gap 1.0mm	$3.00Hz$	$6.25Hz$
gap 2.4mm	$2.50Hz$	$5.25Hz$
System natural frequency (gap $\rightarrow \infty$)	$1.82Hz$	

jump [75] after the maximum impact force in each frequency band. As mentioned, a variation of impact resonance frequency is observed as the gap varies, see Table 2.2. This result was expected [52].

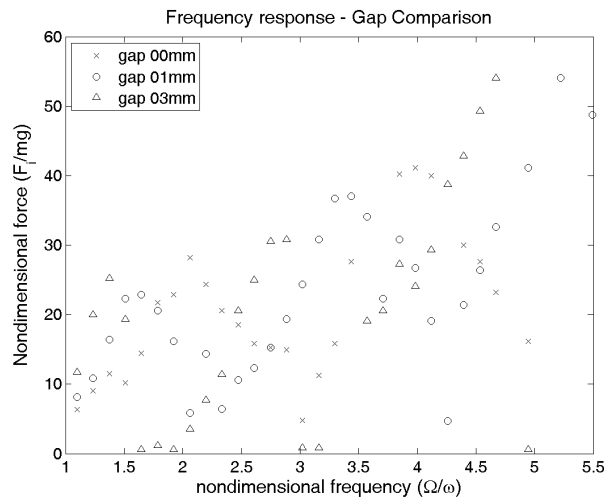


Figure 2.19: Hammer supported by wires. Frequency domain response, non-dimensional force F_i/mg , comparison among gaps.

2.1.7

Nonlinear behavior

The presence of impact and the gap between the hammer and the cart induces nonlinearity, and therefore nonlinear phenomena arise, specifically in the transition between frequency bands. One of these phenomena is the probable change in the basins of attraction for certain excitation frequency/impact gap combinations. In this situation, in which the hammer is excited within a particular frequency but is not impacting the surface, when a small impulse is applied, the hammer starts impacting for some time and returns to the non-impact condition, as shown in Figure 2.20a. However, in some

cases, after the energy is inserted, the system starts impacting and continues in this condition, Figure 2.20b.

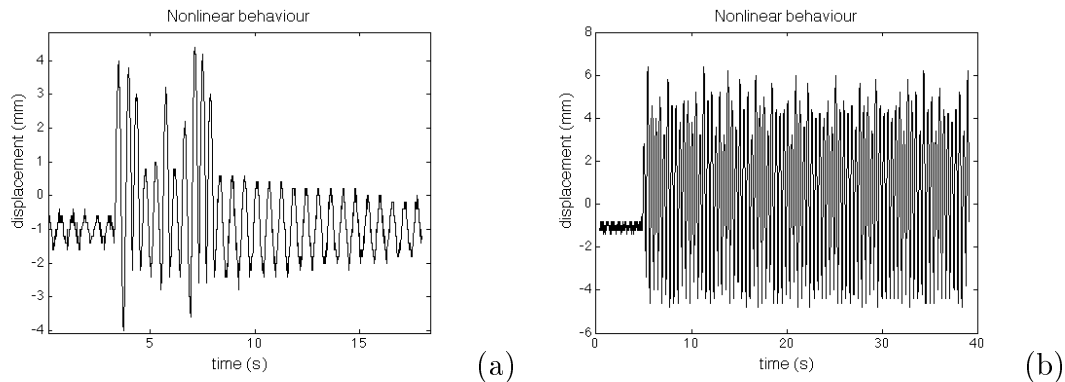


Figure 2.20: Hammer supported by wires. Nonlinear behavior. Hammer displacement over time: a) Condition of no impact/ energy inserted into the system/ system impacts but return to non-impact condition; b) Condition of no impact/ energy inserted into the system/ system impacts and remains in the impact condition.

2.2

Second experiment - hammer supported by beam springs

2.2.1

Experimental apparatus

The experimental apparatus used for experiment two, shown in Figures 2.21, 2.22 and 2.23, is similar to the system presented on the first experiment. It is designed to represent the drillstring axial behavior and its influence on the impact device (hammer). The experiment is also composed of two systems, both moving from the equilibrium position on the horizontal axis.

The first system is exactly the same as in the first experiment, including the low friction rail, the cart and the excitation source (AC motor with off-centered pin and slotted nylon plate). The difference between experiments lies in the hammer. Hammer mass combines an aluminum coupling that holds the springs and the impact device (steel). Hammer stiffness, in contrast to the first experiment, is assured by two clamped-clamped bending beams (steel). These beams have a transverse section of 22.3 mm width and 0.6 mm height. The length of the beams can be changed in order to vary the hammer stiffness. The length of the beams



Figure 2.21: Second test rig.

is defined as the distance between the aluminum couplings (Figure 2.22). As discussed later in this chapter, different values of the hammer stiffness will be determined by changes in the length of the beams. This information will be used to compare different values of hammer stiffness.

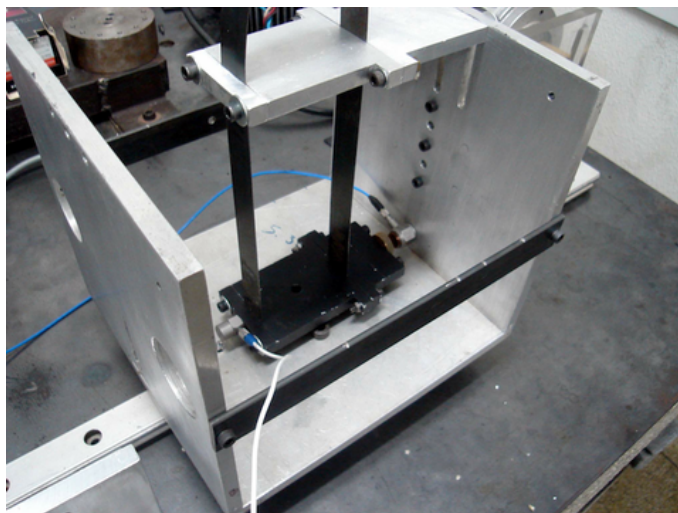


Figure 2.22: Second test rig. Detail of beam springs supporting the hammer

The apparatus used to vary the gap between the hammer and the cart (long screw and a knurled nut) is the same as that used in experiment one, and so are the measuring devices, see Table 2.3.

The methodology is to observe the behavior of the impact system as the gap and the hammer stiffness are varied. In this thesis three different hammer stiffness and three values of gap were chosen, generating nine different possibilities of hammer configurations. For each hammer stiffness, the parameters are identified for the case without impact. Afterwards, a study with impact is carried out. The excitation frequency from the AC motor is varied in order to cover a range of frequencies. The chosen lengths

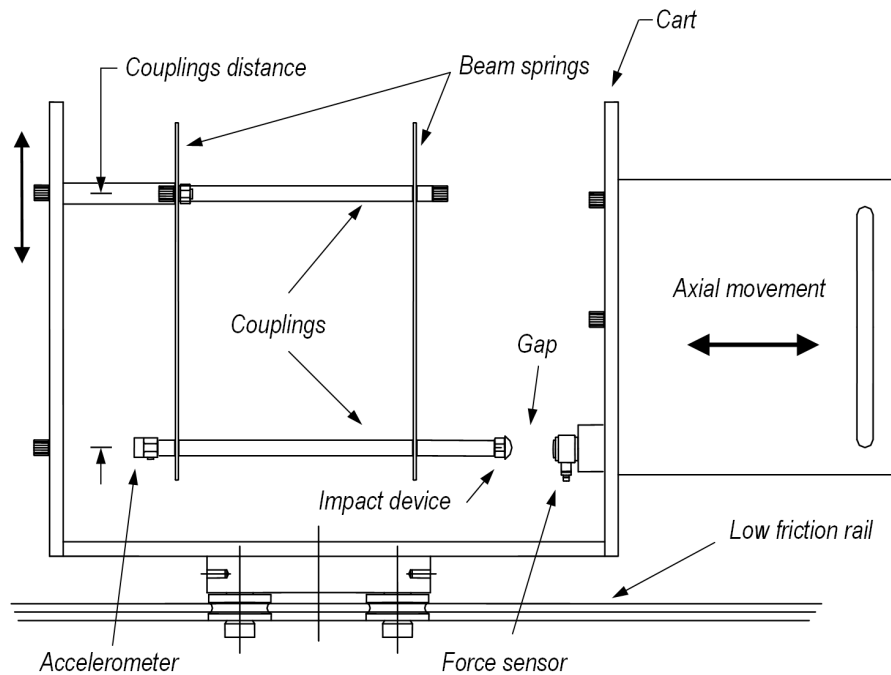


Figure 2.23: Second test rig: experiment sketch.

for the beam springs were 170 mm, 150 mm and 135 mm. Gap lengths studied were 0.0 mm, 1.0 mm and 3.0 mm.

2.2.2

Experimental results for beam spring length 170 mm, gap 0.0 mm

As observed in experiment one, the impact force behavior in this experiment can be divided into frequency bands, showing similar characteristics in each frequency band independent of the gaps, showing a transitory behavior between bands.

For the 0.0 mm gap configuration, the first frequency band is from 4 Hz until 11.5 Hz. This band is characterized by impacts in period-1 (one impact per excitation cycle, or $z = 1/1$). At the lowest excitation frequencies (until 7 Hz), the hammer follows the cart movement, with low magnitudes of impact force. As the excitation frequency increases, the impact force magnitude increases as well, reaching a maximum of 204 N at 9 Hz. After reaching this level, the magnitude of the impact force decreases as the excitation frequency increases. Figure 2.24 shows the impact force and acceleration during impact at low excitation frequency. Figure 2.25 shows the cart and hammer displacements at the same excitation frequency.

Table 2.3: Second experiment. Sensor specs.

Hammer Accelerometer - 751-10 SN AC70		
Sensitivity	10.225	<i>mV/g</i>
Measure Range	± 50	<i>g</i>
Resonance frequency	50	<i>kHz</i>
Impact Force Sensor - PCB 208C03		
Sensitivity	2.263	<i>mV/N</i>
Measure Range	± 2.224	<i>kN</i>
Resonance frequency	75	<i>kHz</i>
Cart laser displacement sensor - optoNCDT 1607-20		
Sensitivity	10	<i>V/mm</i>
Measure Range	20	<i>mm</i>
Hammer laser displacement sensor - optoNCDT 1607-100		
Sensitivity	2	<i>V/mm</i>
Measure Range	100	<i>mm</i>

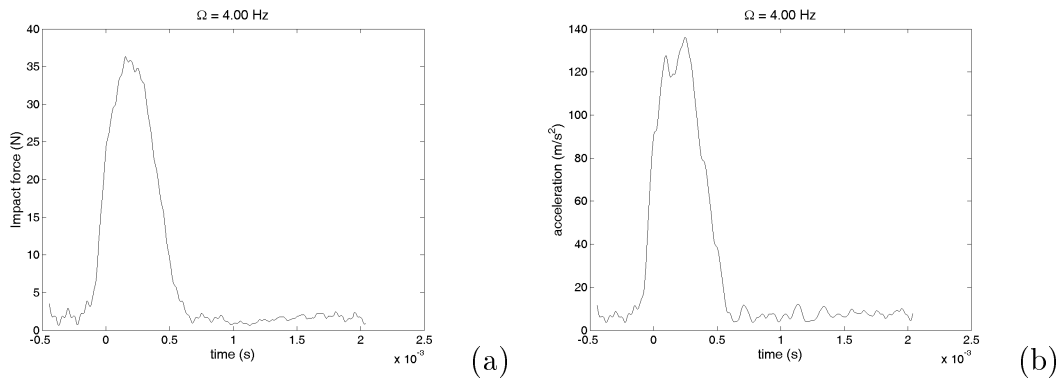


Figure 2.24: Hammer supported by beam springs. Couplings distance 170 mm, gap 0.0 mm. Excitation frequency 4.00 Hz: a) Impact force; b) Hammer acceleration.

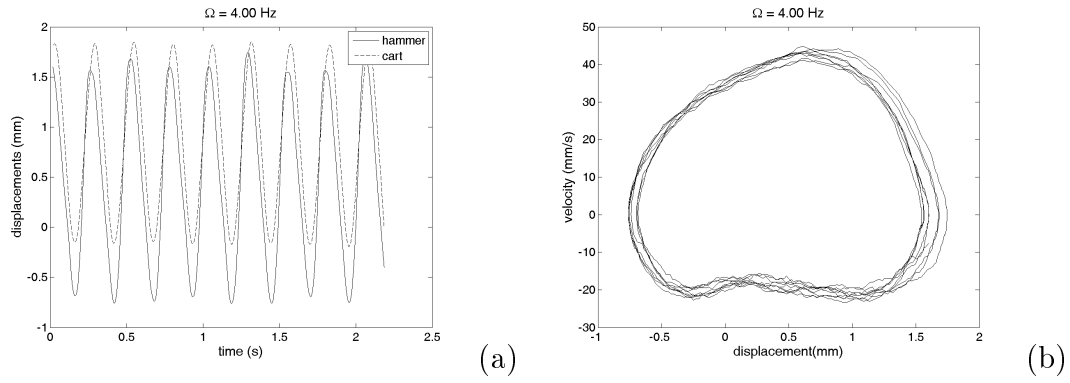


Figure 2.25: Hammer supported by beam springs. Couplings distance 170 mm, gap 0.0 mm. Excitation frequency 4.00 Hz: a) Displacements; b) Hammer phase plane.

Figure 2.26 shows the behavior of the hammer under the maximum impact force in this frequency band ($z = 1/1$).

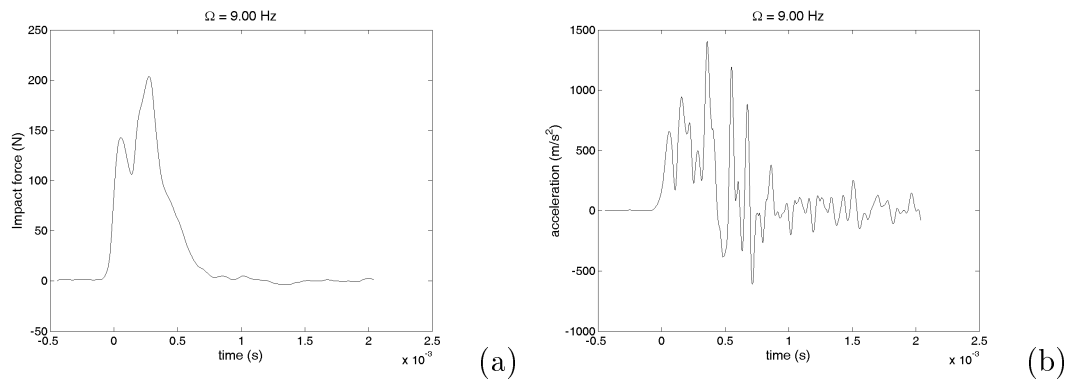


Figure 2.26: Hammer supported by beam springs. Couplings distance 170 mm, gap 0.0 mm. Maximum impact force on the first frequency band. Excitation frequency 9.00 Hz: a) Impact force; b) Hammer acceleration.

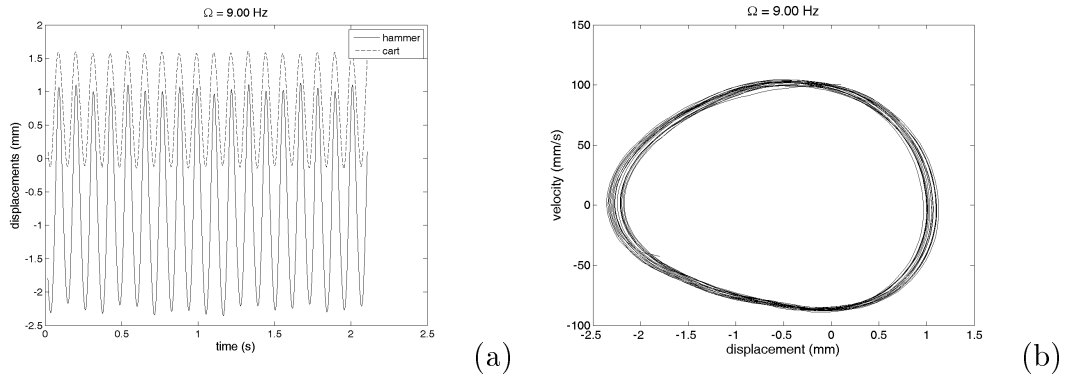


Figure 2.27: Hammer supported by beam springs. Couplings distance 170 mm, gap 0.0 mm. Maximum impact force on the first frequency band. Excitation frequency 9.00 Hz: a) Displacements; b) Hammer phase plane.

After this frequency band, the systems goes through a transitory behavior (bifurcation), characterized by a change in impact characteristics, similar to experiment one. The behavior after the bifurcation is shown in Figure 2.28.

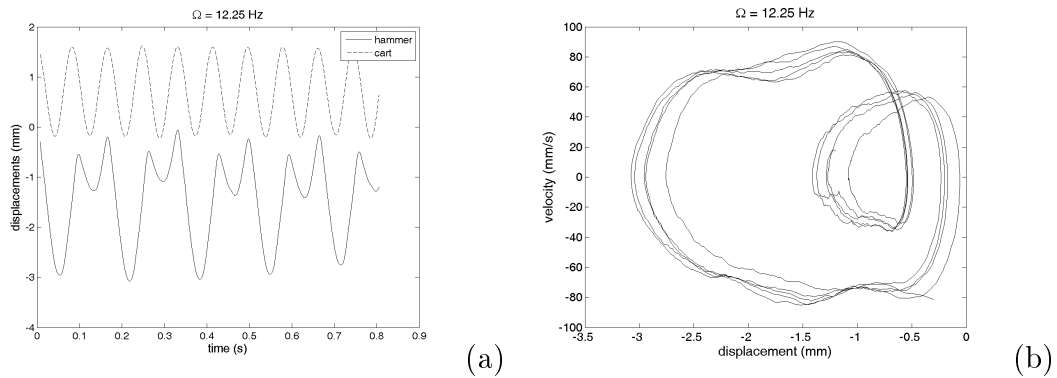


Figure 2.28: Hammer supported by beam springs. Couplings distance 170 mm, gap 0.0 mm. Transitory behavior. Excitation frequency 12.25 Hz: a) Displacements; b) Hammer phase plane.

In the second frequency band, from 12 Hz to 16 Hz, the impacts occur every two cycles of excitation ($z = 1/2$). Because of the high frequencies, the excitation force increases substantially as does the impact force, see equation 2-1. However, for possible field application, the idea is to use the axial vibration of the drillstring to generate the excitation, and this excitation is generally in the low frequency range. Experimental results within frequency band $z = 1/2$ are shown in Figures 2.29 and 2.30.

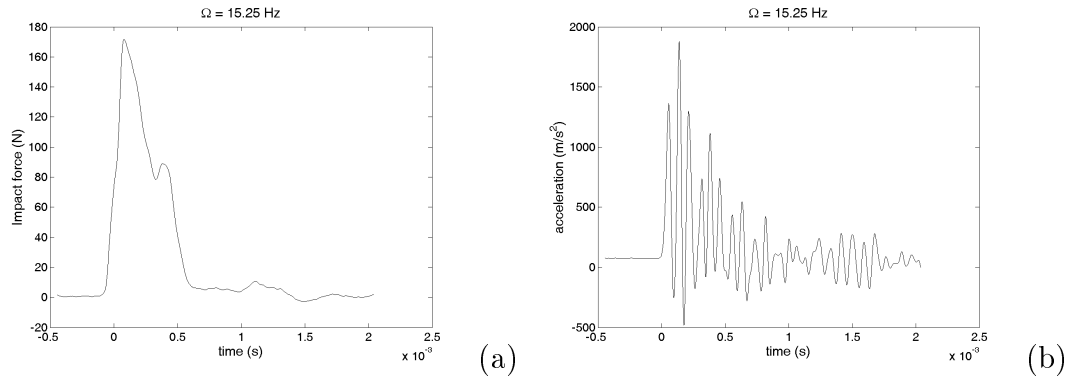


Figure 2.29: Hammer supported by beam springs. Couplings distance 170 mm, gap 0.0 mm. Excitation frequency 15.25 Hz: a) Impact force; b) Hammer acceleration.

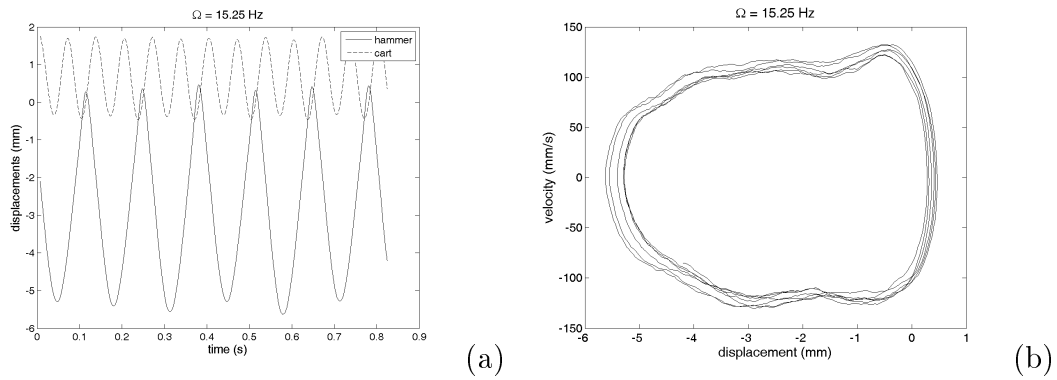


Figure 2.30: Hammer supported by beam springs. Couplings distance 170 mm, gap 0.0 mm. Excitation frequency 15.25 Hz: a) Displacements; b) Hammer phase plane.

At this point it is important to emphasize that, as was observed in experiment one, excitation is not influenced by the impacts, even in conditions of maximum impact force. This is confirmed by the cart displacement under different excitation frequencies.

With this experimental data it is possible to analyze the behavior of the hammer in the frequency domain. The computational routine is the same as applied previously, obtaining the F_i (impact force peak) values for each frequency applied. For this particular stiffness/gap configuration, the impact force ratio chart (F_i/mg) in the frequency domain is shown in Figure 2.31.

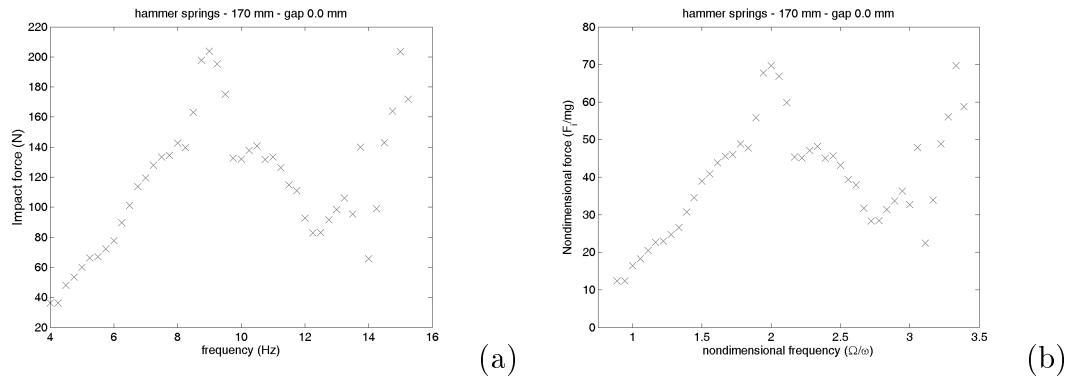


Figure 2.31: Hammer supported by beam springs. Couplings distance 170 mm, gap 0.0 mm. Frequency domain response: a) Maximum impact force; b) non-dimensional force, F_i/mg .

Figure 2.31 shows essentially the same results as found in the first experiment, see Figure 2.11. It is interesting to mention the comparison between the natural frequency of the hammer and the impact resonance. This difference was verified, as observed in experiment one [5] and previous works [52]. The second frequency band is also observed in Figure 2.31, where the impact force magnitude is higher because of an increase in excitation energy. However, comparing these values in non-dimensional terms (Figure 2.31(b)) the second frequency band does not generate significant impacts when compared with the first frequency band, remembering that the amount of energy inserted into the hammer increases with the square of the excitation frequency, see equation (2-1).

2.2.3

Experimental results for beam spring length 170 mm, gaps 1.0 mm and 3.0 mm

Similar to the results obtained for gap 0.0 mm configuration, the hammer response for 1.0 mm and 3.0 mm gap configurations may also be separated into frequency bands. Some differences are observed in these non-zero gap conditions as compared to 0.0 mm gap condition. For instance, the occurrence of nonlinear jump after the impact resonance. Another difference is the occurrence of conditions of no impact at higher excitation frequencies.

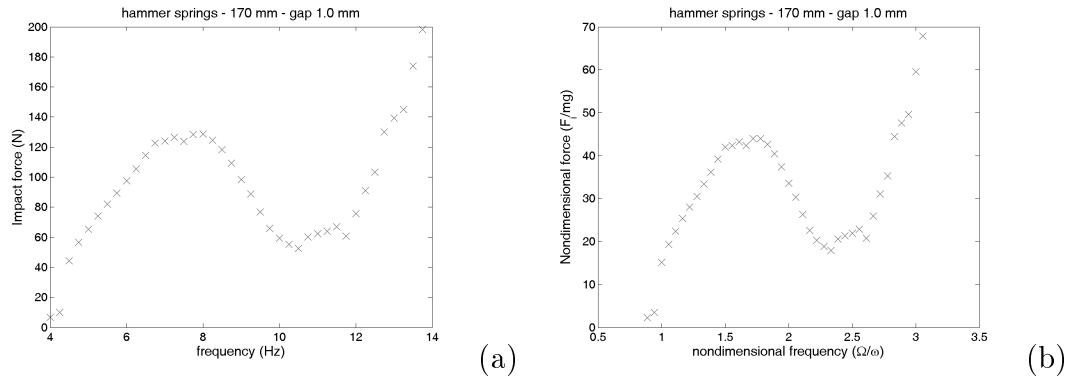


Figure 2.32: Hammer supported by beam springs. Couplings distance 170 mm, gap 1.0 mm. Frequency domain response: a) Maximum impact force; b) non-dimensional force, F_i/mg .

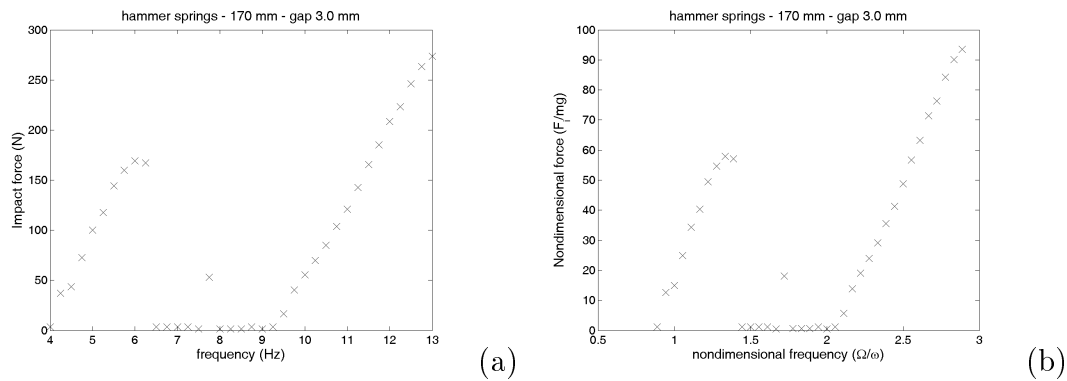


Figure 2.33: Hammer supported by beam springs. Couplings distance 170 mm, gap 3.0 mm. Frequency domain response: a) Maximum impact force; b) non-dimensional force, F_i/mg .

2.2.4

Experimental results for beam spring length 150 mm

For this hammer stiffness, the same gaps were used (0.0 mm, 1.0 mm and 3.0 mm), and the same frequency band pattern was observed. Due to a smaller beam spring length (consequently a higher value of hammer stiffness) higher impact resonance frequencies are found for each stiffness/gap configuration. The test rig shows a limitation at higher excitation frequencies. When the excitation frequency reaches 12 Hz or more, the vibration levels on the mounting structure supporting the AC motor become substantially higher. This vibration level is transmitted to the rest of the test rig (low friction rail, cart and hammer). At a certain point as hammer

stiffness increases, data acquisition becomes impossible. This vibration level can be measured partially by cart displacement. Figure 2.34 shows the maximum cart displacement amplitude for each excitation frequency for beam spring length of 150 mm and 1.0 mm impact gap.

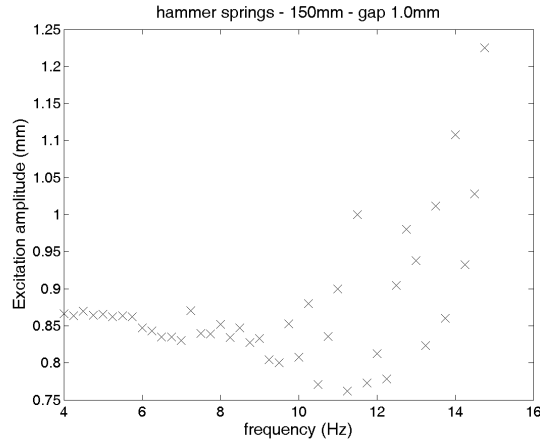


Figure 2.34: Hammer supported by beam springs. Couplings distance 150 mm, gap 1.0 mm. Cart displacement amplitude *versus* excitation frequency.

Following figures show the output parameters (impact force, hammer acceleration, hammer and cart displacements) and hammer phase plane, within each frequency band, for all gaps used (where this was possible, given test rig limitation).

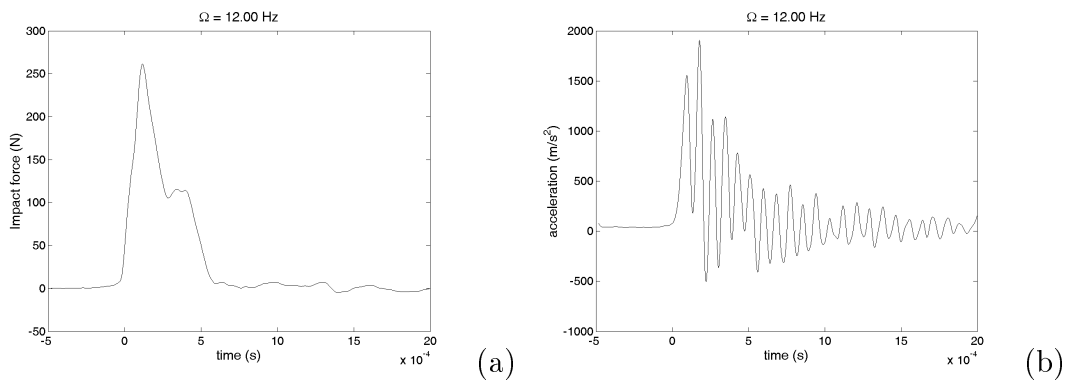


Figure 2.35: Hammer supported by beam springs. Couplings distance 150 mm, gap 0.0 mm. Excitation frequency 12.00 Hz: a) Impact force; b) Hammer acceleration.

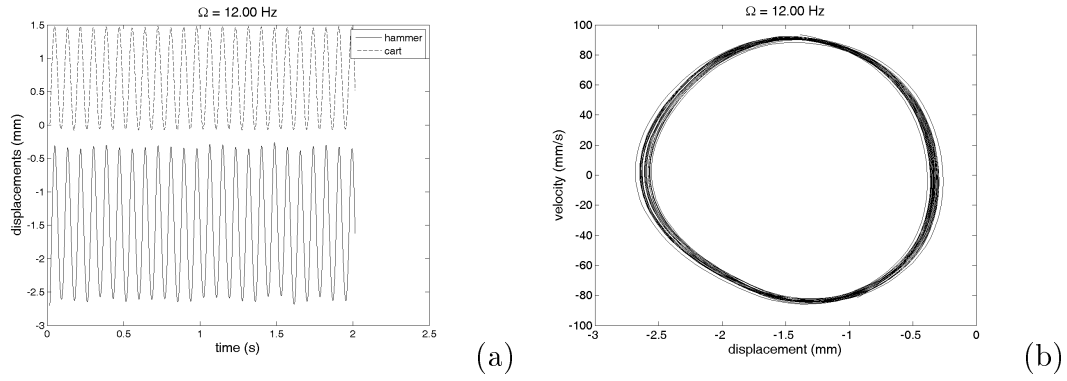


Figure 2.36: Hammer supported by beam springs. Couplings distance 150 mm, gap 0.0 mm. Excitation frequency 12.00 Hz: a) Displacements; b) Hammer phase plane.

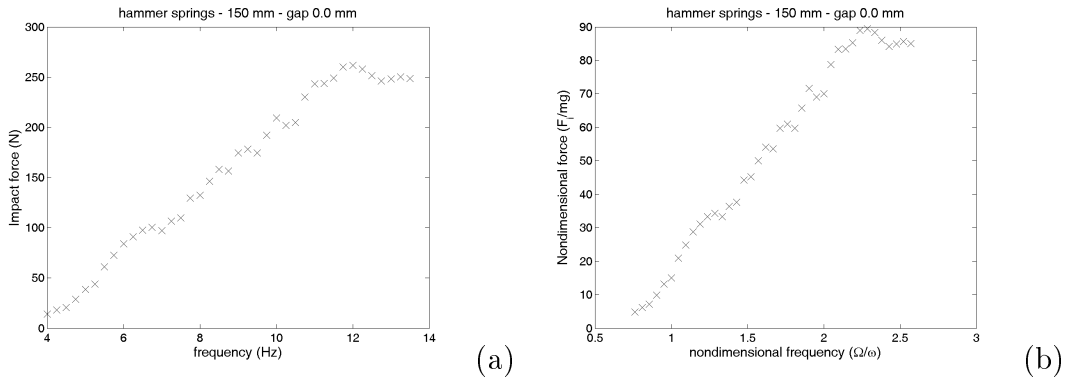


Figure 2.37: Hammer supported by beam springs. Couplings distance 150 mm, gap 0.0 mm. Frequency domain response: a) Maximum impact force; b) non-dimensional force, F_i/mg .

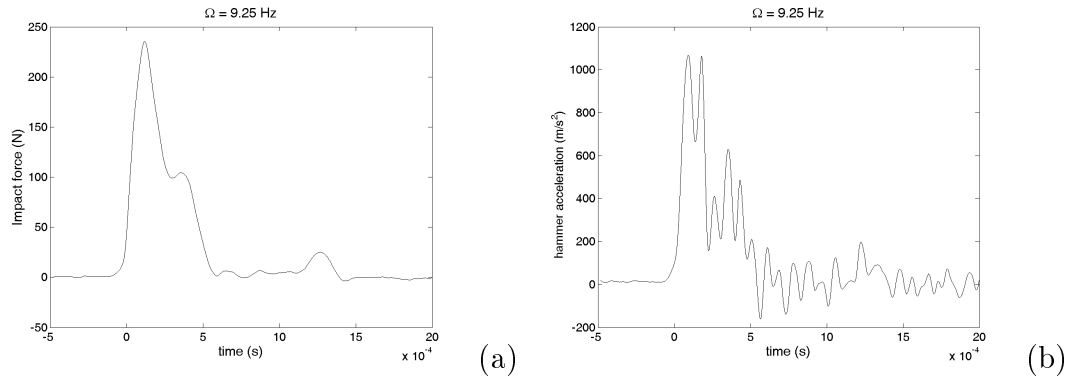


Figure 2.38: Hammer supported by beam springs. Couplings distance 150 mm, gap 1.0 mm. Excitation frequency 9.25 Hz: a) Impact force; b) Hammer acceleration.

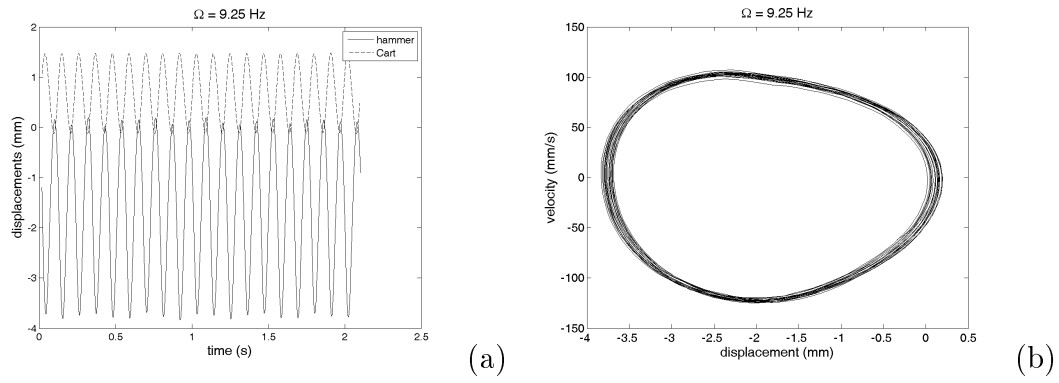


Figure 2.39: Hammer supported by beam springs. Couplings distance 150 mm, gap 1.0 mm. Excitation frequency 9.25 Hz: a) Displacements; b) Hammer phase plane.

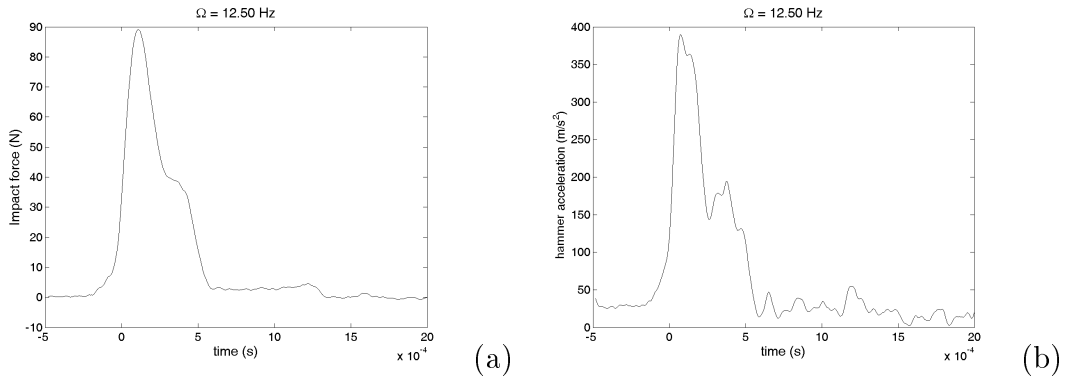


Figure 2.40: Hammer supported by beam springs. Couplings distance 150 mm, gap 1.0 mm. Excitation frequency 12.50 Hz: a) Impact force; b) Hammer acceleration.

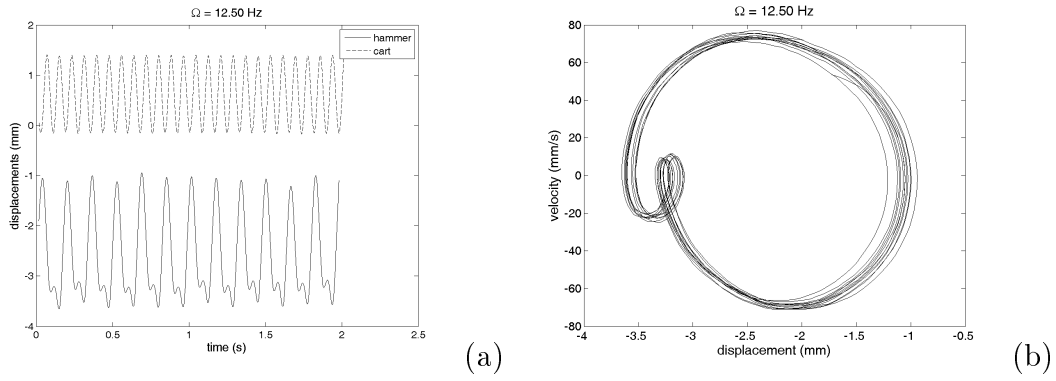


Figure 2.41: Hammer supported by beam springs. Couplings distance 150 mm, gap 1.0 mm. Excitation frequency 12.50 Hz: a) Displacements; b) Hammer phase plane.

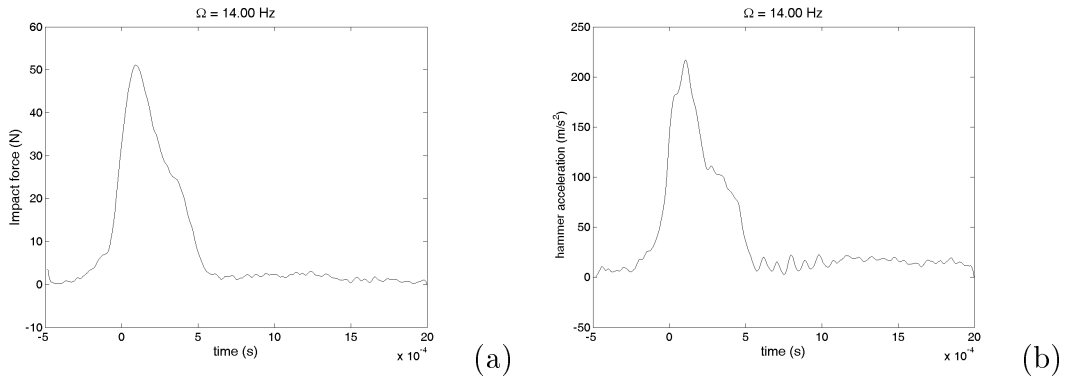


Figure 2.42: Hammer supported by beam springs. Couplings distance 150 mm, gap 1.0 mm. Excitation frequency 14.00 Hz: a) Impact force; b) Hammer acceleration.

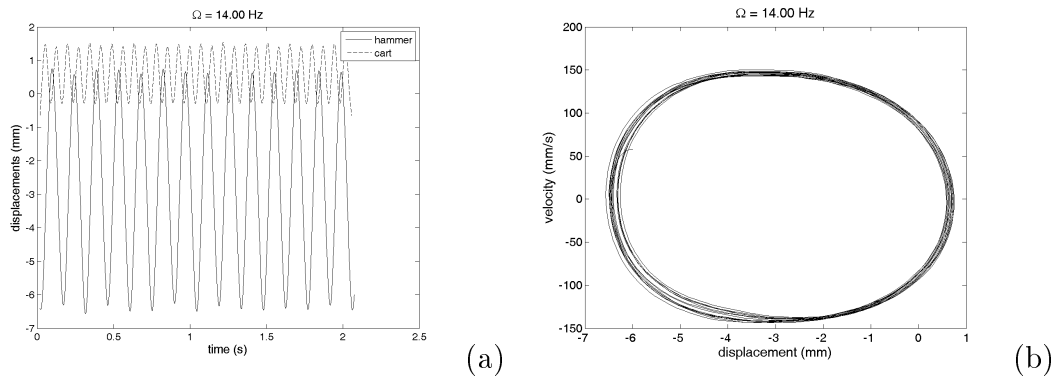


Figure 2.43: Hammer supported by beam springs. Couplings distance 150 mm, gap 1.0 mm. Excitation frequency 14.00 Hz: a) Displacements; b) Hammer phase plane.

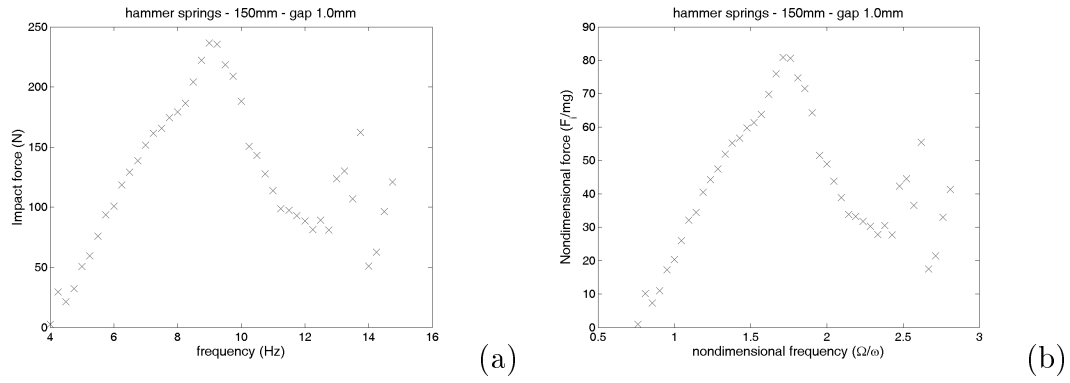


Figure 2.44: Hammer supported by beam springs. Couplings distance 150 mm, gap 1.0 mm. Frequency domain response: a) Maximum impact force; b) non-dimensional force, F_i/mg .

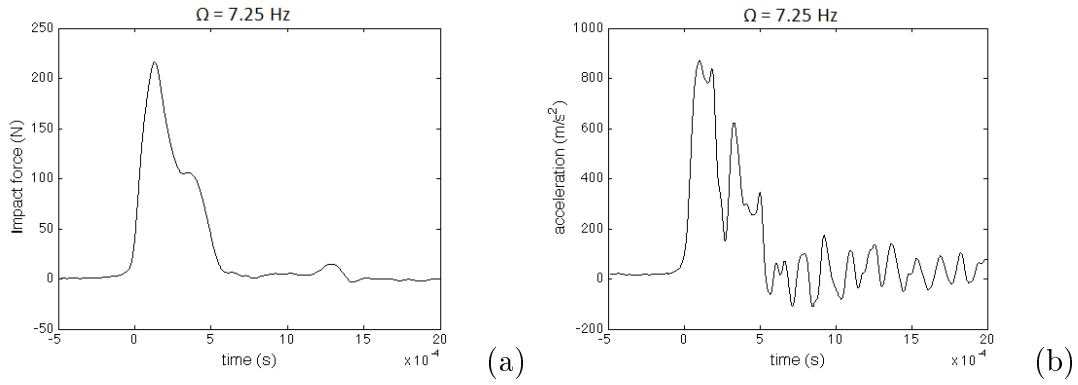


Figure 2.45: Hammer supported by beam springs. Couplings distance 150 mm, gap 3.0 mm. Excitation frequency 7.25 Hz: a) Impact force; b) Hammer acceleration.

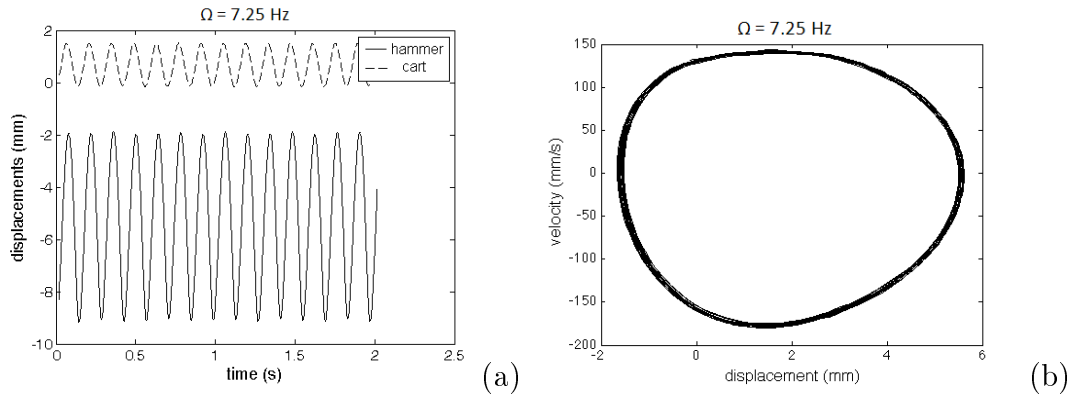


Figure 2.46: Hammer supported by beam springs. Couplings distance 150 mm, gap 3.0 mm. Excitation frequency 7.25 Hz: a) Displacements; b) Hammer phase plane.

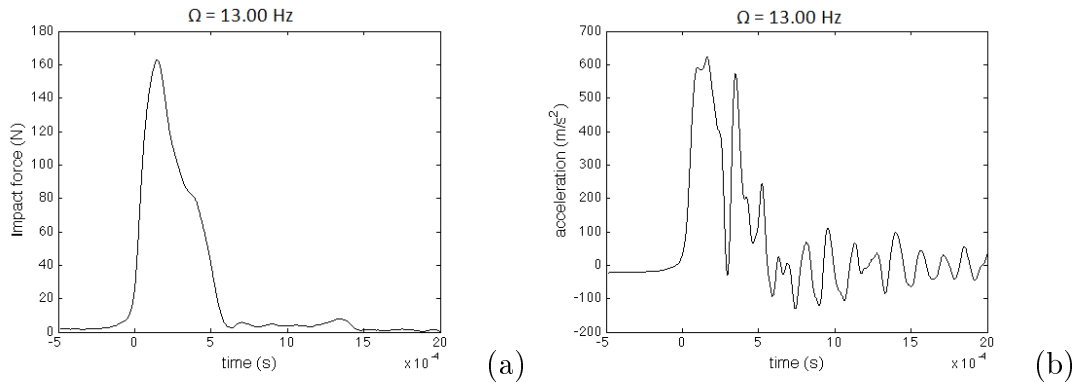


Figure 2.47: Hammer supported by beam springs. Couplings distance 150 mm, gap 3.0 mm. Excitation frequency 13.00 Hz: a) Impact force; b) Hammer acceleration.

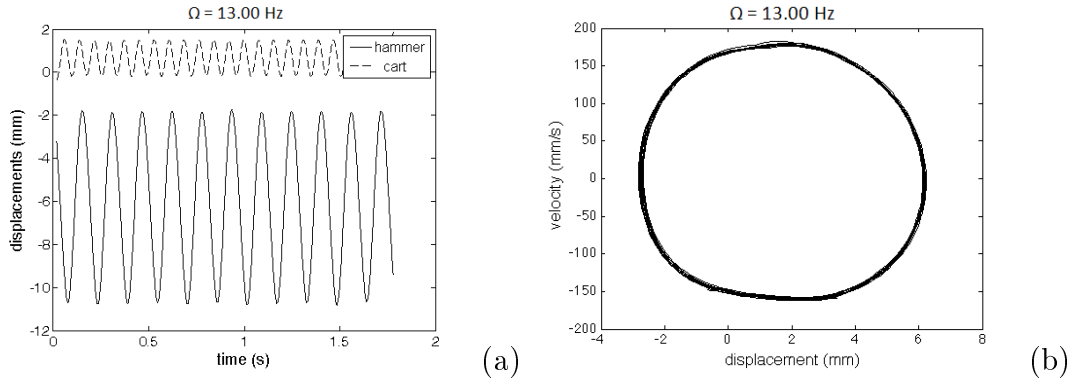


Figure 2.48: Hammer supported by beam springs. Couplings distance 150 mm, gap 3.0 mm. Excitation frequency 13.00 Hz: a) Displacements; b) Hammer phase plane.

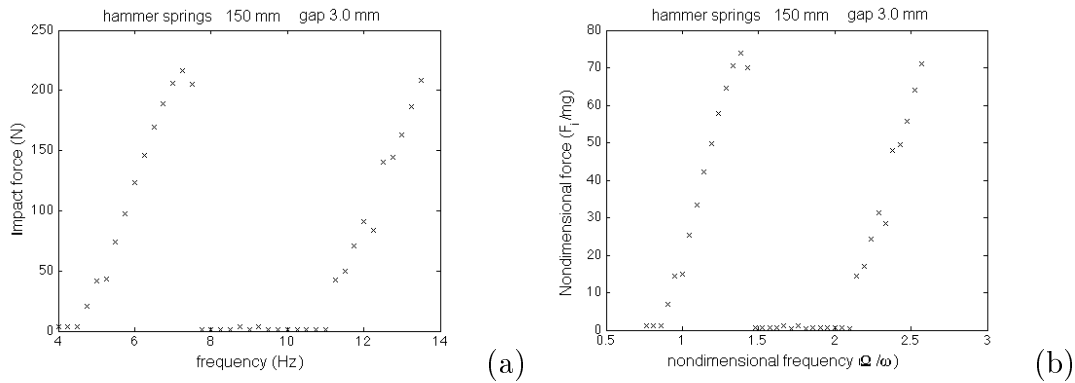


Figure 2.49: Hammer supported by beam springs. Couplings distance 150 mm, gap 3.0 mm. Frequency domain response: a) Maximum impact force; b) non-dimensional force, F_i/mg .

2.2.5 Experimental results for beam spring length 135 mm

The impact force behavior of this hammer stiffness follows the same patterns already observed, regardless of the gap imposed. For the 0.0 mm gap configuration, it was not possible to identify the impact resonance frequency ($z = 1/1$), because the frequency was out of the test rig range measuring capability. For the other gap configurations, 1.0 mm and 3.0 mm, the impact resonance frequency was observed. No data on frequency band $z = 1/2$ was obtained due to test rig limitation. The nonlinear jump after the impact resonance was observed for the 3.0 mm gap configuration but it was not observed for the 1.0 mm gap.

Because the impact force pattern is similar to previous experiments, charts documenting the outputs are omitted. Figures 2.50, 2.51 and 2.52 show the impact force and the non-dimensional force (F_i/mg) in the frequency domain for the 3 gap configurations.

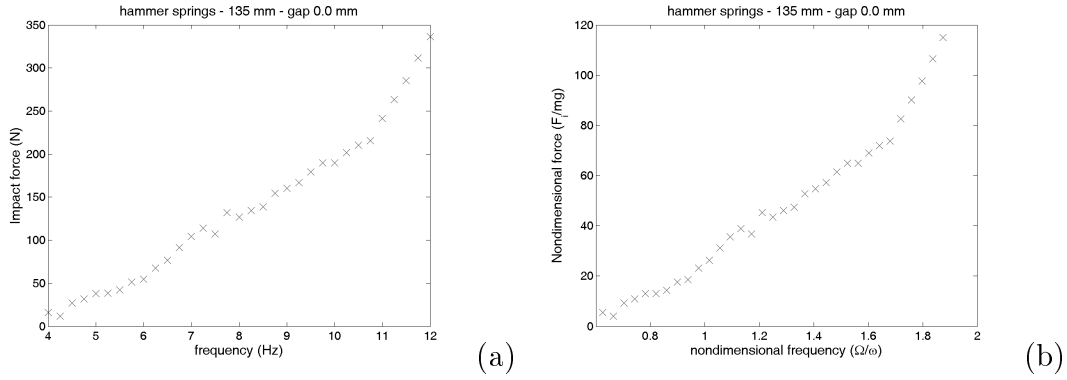


Figure 2.50: Hammer supported by beam springs. Couplings distance 135 mm, gap 0.0 mm. Frequency domain response: a) Maximum impact force; b) non-dimensional force, F_i/mg .

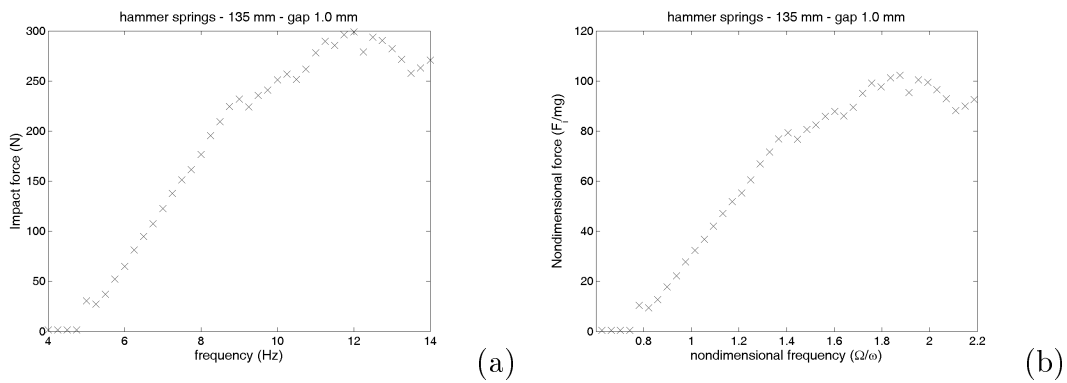


Figure 2.51: Hammer supported by beam springs. Couplings distance 135 mm, gap 1.0 mm. Frequency domain response: a) Maximum impact force; b) non-dimensional force, F_i/mg .

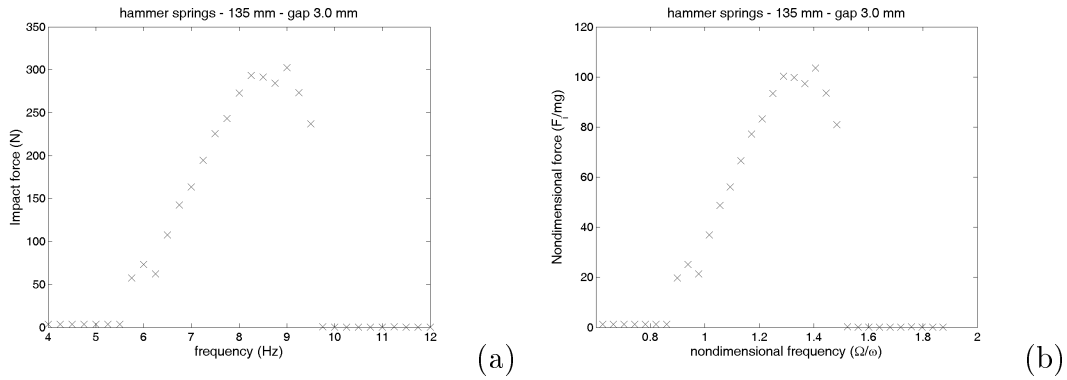


Figure 2.52: Hammer supported by beam springs. Couplings distance 135 mm, gap 3.0 mm. Frequency domain response: a) Maximum impact force; b) non-dimensional force, F_i/mg .

2.2.6 Comparison between stiffness/ gap configurations

From the experimental analysis presented in this section, it is possible to compare the impact force under different situations. First, the impact force behavior is analyzed in terms of the gap, for the same value of hammer stiffness. The charts are shown in Figures 2.53, 2.54 and 2.55, for hammer beam springs lengths of (stiffness) 170 mm, 150 mm and 135 mm, respectively.

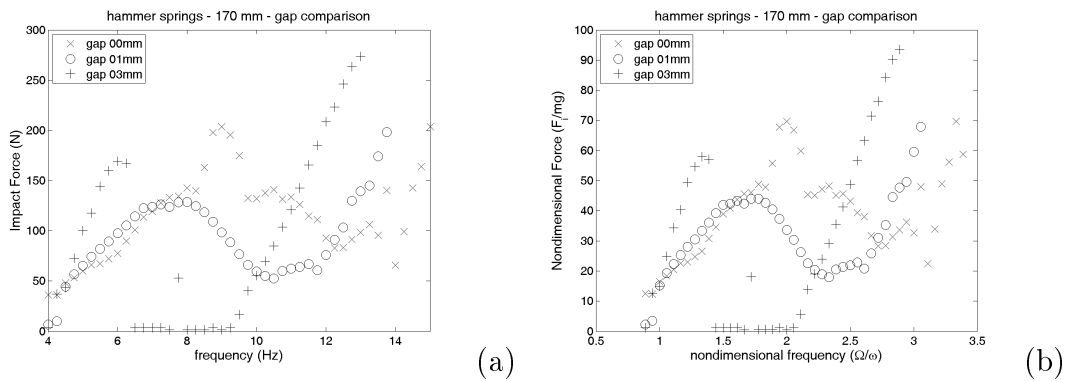


Figure 2.53: Hammer supported by beam springs. Couplings distance 170 mm; comparison among gaps. Frequency domain response: a) Maximum impact force; b) non-dimensional force, F_i/mg .

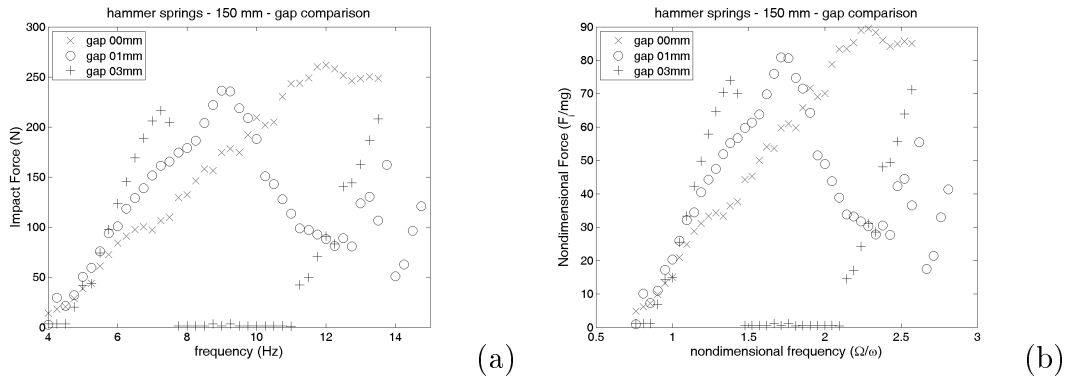


Figure 2.54: Hammer supported by beam springs. Couplings distance 150 mm; comparison among gaps. Frequency domain response: a) Maximum impact force; b) non-dimensional force, F_i/mg .

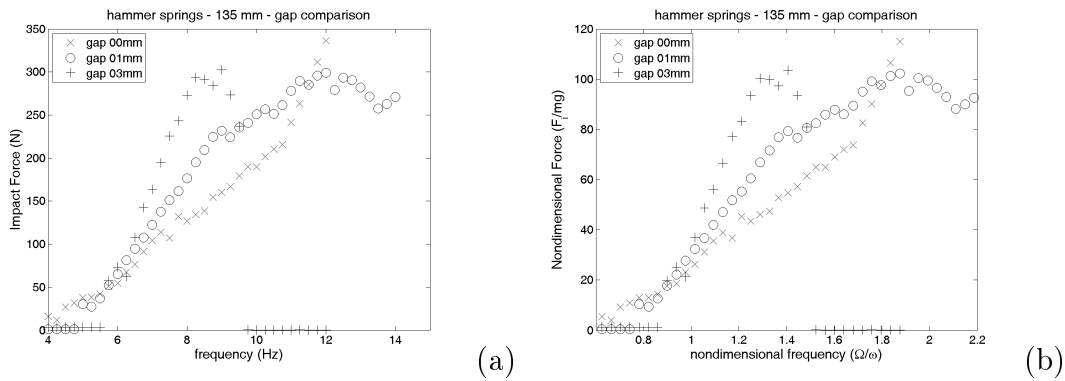


Figure 2.55: Hammer supported by beam springs. Couplings distance 135 mm; comparison among gaps. Frequency domain response: a) Maximum impact force; b) non-dimensional force, F_i/mg .

For beam spring length of 170 mm, the highest impact force is observed for the 0.0 mm gap configuration, which had an impact force of 70 times the weight of the hammer. Expectations are that the hammer behavior for gap 1.0 mm configuration should be in between 0.0 mm and 3.0 mm gap configurations, with similar non-dimensional maximum force value, see Figure 2.53. This expected behavior is verified in other configurations (150 mm and 135 mm beam spring length) but not in the 170 mm beam spring length. Observing the impact force behavior for the 3.0 mm gap configuration, it can be seen that although the second frequency band develops higher impact forces, such results are not significant when compared in non-dimensional terms, as previously explained.

The comparison between gap configurations for beam spring lengths of 150 mm and 135 mm, see Figures 2.54 and 2.55, shows the same variation of impact resonance. As verified previously, the highest value of the impact force is observed in the 0.0 mm gap configuration. When the non-dimensional force is analyzed, all configurations show the maximum impact force at the same level. For beam spring length of 135 mm, it was not possible to determine the maximum impact force and corresponding impact resonance, because of test rig limitation.

For possible use in the field, it is recommended the hammer operates within the frequency band $z = 1/1$ (one impact per excitation cycle), using the 0.0 mm gap. This configuration possesses more stability, in other words, a variation of the excitation frequency around the impact resonance results in a small variation of impact force, with no occurrence of nonlinear jump.

Other possible comparison can be made by maintaining the same value of the gap and changing the hammer stiffness. This is shown in Figures 2.56, 2.57 and 2.58.

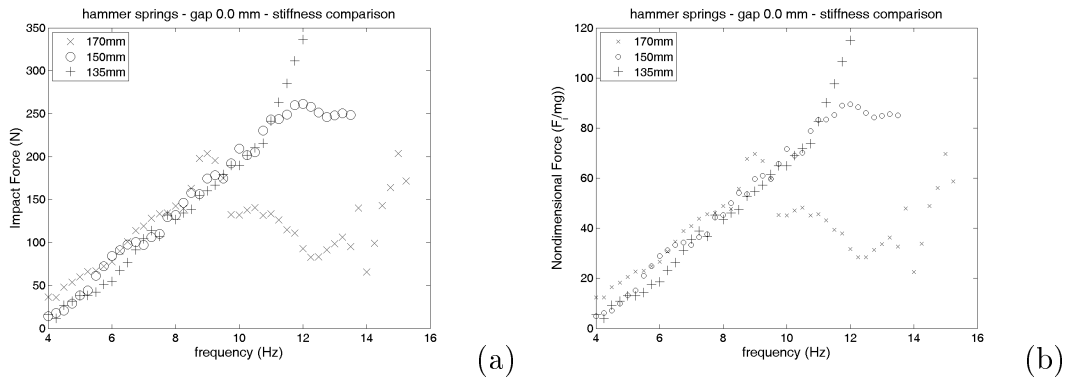


Figure 2.56: Hammer supported by beam springs. Gap 0.0 mm; comparison among stiffness. Frequency domain response: a) Maximum impact force; b) non-dimensional force, F_i/mg .

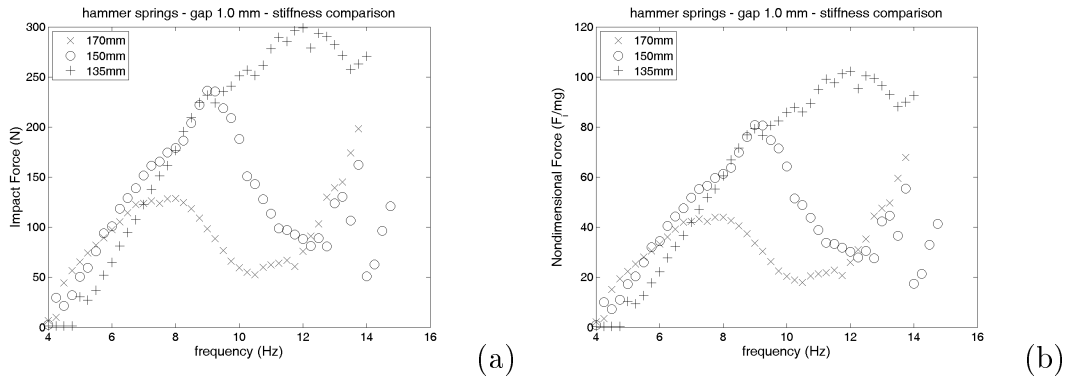


Figure 2.57: Hammer supported by beam springs. Gap 1.0 mm; comparison among stiffness. Frequency domain response: a) Maximum impact force; b) non-dimensional force, F_i/mg .

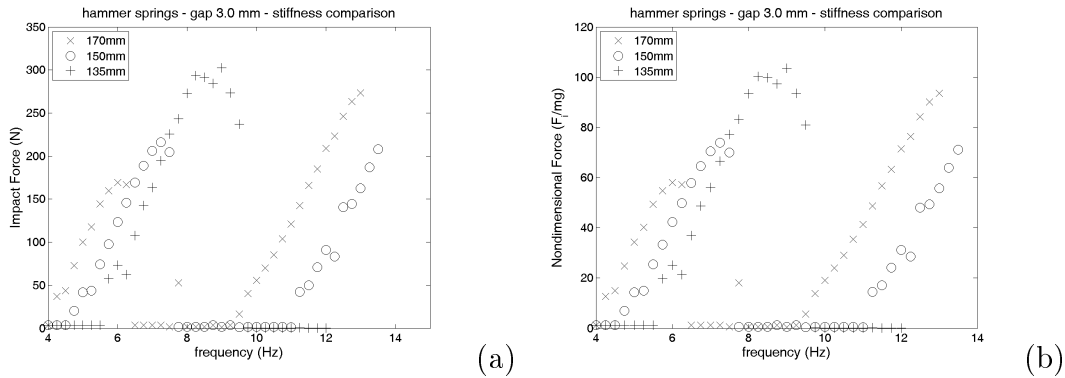


Figure 2.58: Hammer supported by beam springs. Gap 3.0 mm; comparison among stiffness. Frequency domain response: a) Maximum impact force; b) non-dimensional force, F_i/mg .

Regardless of the gap imposed on the hammer, higher impact forces are achieved with higher hammer stiffness, see Figures 2.56, 2.57 and 2.58. The change in hammer stiffness creates a change in the impact resonance. However this is not an RHD parameter, because the excitation frequency comes from the drilling process (drill string rotary motion). Because the drilling rotation speed in the field is defined, the one variable that affects the maximum impact force is hammer stiffness.

One interesting fact to be considered is that, for the same gap configuration, the values of the impact force in the low range of frequency band $z = 1/1$ are the same regardless of hammer stiffness.

Finally, Table 2.4 shows the impact resonance in frequency band $z = 1/1$, as well as the impact force magnitude.

Table 2.4: Impact resonance frequencies and impact force magnitudes (experimental), frequency band $z = 1/1$.

Beam spring length/ gap	Frequency (Hz)	F_i (N)	F_i/mg
170 mm			
gap 0.0mm	9.00	203.6	70
gap 1.0mm	7.75	128.6	44
gap 2.4mm	6.00	169.5	58
No impact (gap $\rightarrow \infty$)	4.50	–	–
150 mm			
gap 0.0mm	12.00	261.6	89
gap 1.0mm	9.00	236.4	74
gap 2.4mm	7.25	216.2	81
No impact (gap $\rightarrow \infty$)	5.25	–	–
135 mm			
gap 0.0mm	?	?	?
gap 1.0mm	12.00	299.1	102
gap 2.4mm	9.00	302.5	104
No impact (gap $\rightarrow \infty$)	6.50	–	–

2.2.7

Hammer modal analysis

In previous works [3] [4] [5], the comparison between experimental data and numerical simulation has delivered unsatisfactory results, when the mathematical modeling used rigid body dynamics to describe the hammer behavior. According to the common impact force profile it seems that the cart plate where the impact force sensor is mounted adds a factor of flexibility, see Figure 2.22. This is verified by the two peaks in impact force chart. This subject will be further discussed in Chapter 3.

To better understand the hammer dynamics, a modal analysis is performed, where the natural frequencies of the hammer with the beam springs are determined. The experiment is equipped with an extra mini accelerometer (Endevco 25B, SN BL55, sensitivity 4.7707 mv/g), located on one of the beam springs at the end closest to the hammer. The idea is to separate the frequency response function of the hammer from the beam springs. The impact force signal is used as the trigger and the FRF is obtained during the hammer motion following the impact. Two separate tests are performed. For each test the triggered signal is obtained by averaging data from 5 trials. Results are shown in Figures 2.59 and 2.60, for beam spring lengths of 170 mm and 150 mm, respectively.

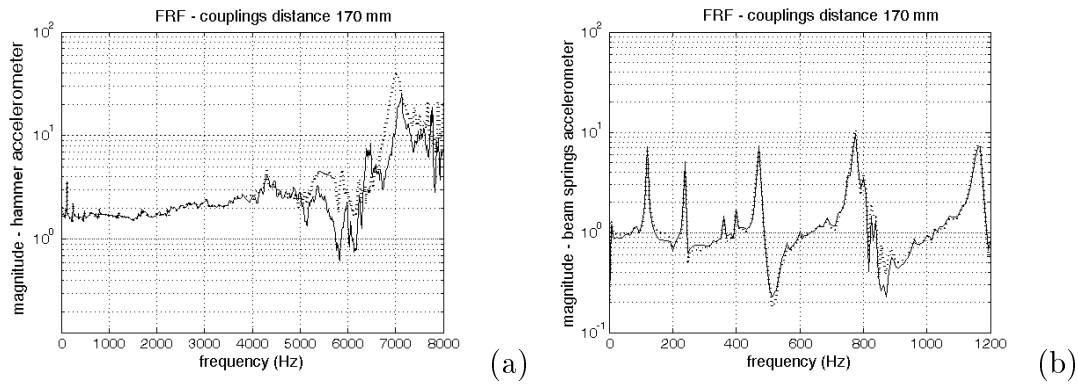


Figure 2.59: Frequency domain response in free flight after impact. Couplings distance 170 mm: a) Hammer accelerometer; b) Beam spring accelerometer.

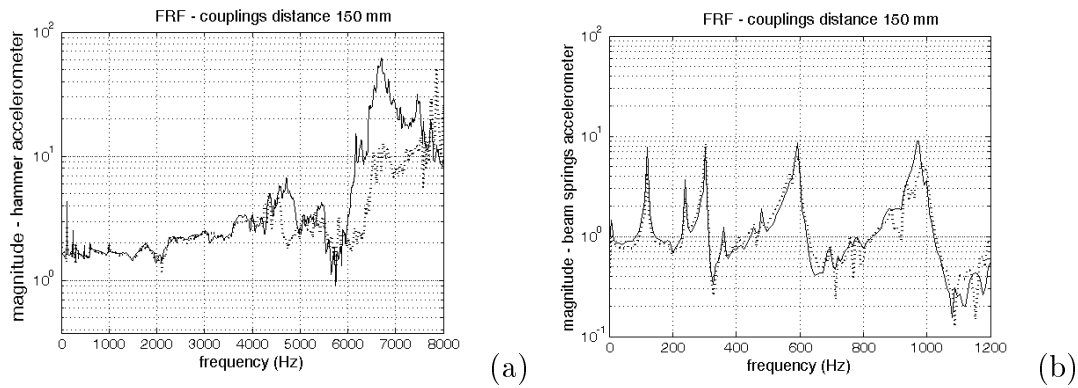


Figure 2.60: Frequency domain response in free flight after impact. Couplings distance 150 mm: a) Hammer accelerometer; b) Beam spring accelerometer.

After impact the beam springs behave like a clamped-clamped beam in bending vibration. Analyzing the FRFs, as shown in Figures 2.59(a) and 2.60(b), several peaks in the low frequency range are observed. These frequencies are associated to the first bending vibration modes of the beam springs. Also, a peak in the high frequency range is detected (around 7000 Hz). This frequency is associated to the axial vibration of the hammer itself.

To understand the hammer axial behavior, the FFT of the original acceleration signal for the hammer supported by wires was obtained, see Figure 2.2. Several trials were performed and the results are shown in Figure 2.61.

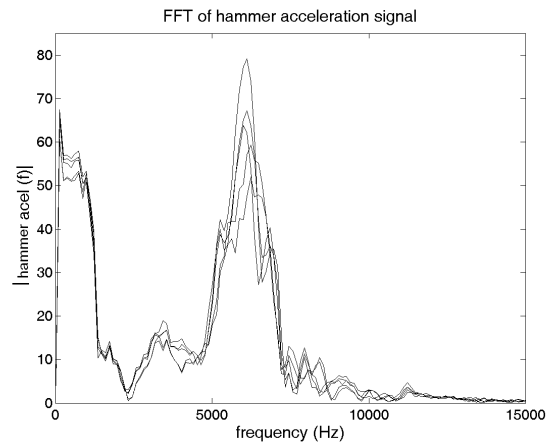


Figure 2.61: Hammer supported nylon wires. FFT of several acceleration signals at moment of impact.

The Fourier Transform of the hammer acceleration following impact reveals three peaks, shown in Figure 2.61. The first peak, in the 1 kHz range, can be associated to the envelope of the acceleration signal. The second peak at around 3 kHz has a lower magnitude. This peak is associated to the impact force profile. The last peak occurs at around 6 kHz, and corresponds to the axial oscillations after impact.

2.3

Impact force comparison between experiments

When comparing the magnitudes of the impact force from both experiments, it is observed that the second test rig configuration (hammer supported by beam springs) generates higher impact forces of significant value (factor 3 minimum), regardless of the stiffness imposed by the beam springs. This can be explained by the fact that beam springs have the capability of storing potential energy, increasing overall energy of the hammer and, consequently, generating higher impact forces.

When the non-dimensional frequencies are compared, regardless of what is supporting the hammer (wires or beam springs), it seems that system impact resonance is a function of the gap, not depending on the stiffness, see Table 2.5.

Table 2.5: Non-dimensional impact resonance frequencies (Ω/ω), all hammer configurations, frequency band $z = 1/1$.

gap (mm)	hammer wires	hammer springs 135 mm	hammer springs 150 mm	hammer springs 170 mm
0.0	2.1	?	2.2	2.0
1.0	1.6	1.8	1.7	1.7
2.4	1.4	–	–	–
3.0	–	1.4	1.4	1.3

2.4

Final remarks

The purpose of this chapter was to present the experimental investigation of the impact force behavior in a vibro-impact system, where a hammer is embarked on a cart that moves by a prescribed oscillatory displacement. By changing the hammer characteristics and the impact gap it is possible to investigate the impact force behavior under different excitation frequencies. Two similar experiments were performed, in order to isolate and decouple the phenomena involved. This allows for a better understanding of each phenomenon separately. These test rigs were an improvement on an earlier test rig. The new test rig changed some important configurations and used new measuring hardware and sensors, capable of capturing the impact phenomenon in a more precise time scale, to provide more information on the impact force itself.

In both experiments it was noted that, in all stiffness/ gap combinations, there was a certain pattern of the impact force behavior. This could be divided into frequency bands, showing similar characteristics in each frequency band for all configurations. In each frequency band, impact force behavior has a regular pattern, while in frequency band transitions the hammer shows some nonlinear behavior.

The presence of the gap significantly changes the impact resonance as compared to its natural frequency.

Concerning the phase plane charts, a smoothing effect during the impact was observed. This is caused by the differentiation of the low-pass filtered signal. It does not reflect the reality of the impact, as it will be seen during the comparison between experimental data and numerical simulations.

For possible use in the field, it is recommended to operate the hammer within in the first impact resonance (frequency band $z = 1/1$), using a gap

of 0.0 mm, because this configuration offers more stability.

To help develop an improved mathematical model, a modal analysis of the hammer was performed. Following the impact, the beam springs presented the behavior of a clamped-clamped beam in bending vibration. Some peaks in the high frequency range of the hammer FRF were observed. These frequencies are associated with the axial vibration of the hammer itself and the contact dynamics.

When comparing the magnitudes of the impact force from both experiments, it is observed that the second test rig (hammer supported by springs) generates significantly higher impact forces, regardless of the stiffness imposed by the beam springs.